Chapter 20

Interpretation of Marine CSEM and Marine MT Data for Hydrocarbon Prospecting

Ståle Emil Johansen and Pål T. Gabrielsen

20.1 Introduction

Remote sensing techniques record variations in petrophysical parameters such as acoustic or electric properties. Seismic sounding is by far the most common of such tools. Seismic techniques can detect strata and structure in the subsurface that are potential hydrocarbon (HC) traps. By interpreting the seismic a detailed geological model can be constructed, but seismic data has limitations in direct prediction of pore fluid composition. Given detection of a structural geometry that may contain HC within porous sedimentary rocks, the main remaining uncertainty is normally whether the pore space is filled with saline water or HC. For this reason only 10–30% of exploration wells penetrate commercial oil or gas reserves in many areas.

Controlled source electromagnetic (CSEM) data has been used for several years for general mapping of electrical properties of the subsurface. In the late 1990s Statoil scientists Svein Ellingsrud, Terje Eidesmo and Ståle Johansen developed the use of the CSEM method for remote identification of hydrocarbons in a marine setting. The early tests of the method were positive and in co-operation with NGI, Statoil established EMGS that further developed and commercialised the CSEM technique for hydrocarbon exploration.

S.E. Johansen (✉)
NTNU, Trondheim, Norway
e-mail: stale.johansen@ntnu.no

P.T. Gabrielsen
EMGS (ElectroMagnetic GeoServices ASA), Trondheim, Norway
e-mail: ptg@emgs.com

Controlled source electromagnetic (CSEM) sounding uses EM energy transmitted by a horizontal electric dipole (HED) source to detect contrasts in subsurface resistivity. Although EM techniques have been used for many years, detection of subsurface hydrocarbons by CSEM sounding is still a new discipline within HC prospecting.

A full scale CSEM sounding research test was first done offshore Angola in 2000 by Statoil, and showed that the CSEM technique could detect deeply buried hydrocarbons. The first commercial test was done in 2002 by EMGS on the Ormen Lange Field offshore Norway. For some time the interpretation of CSEM data was hampered by the lack of statistically significant calibration data demonstrating that deeply buried HC accumulations were detectable by the method. However, development of new equipment opened the way for improved acquisition, processing and interpretation of CSEM data, and in 2003 the Troll CSEM data was collected by EMGS. This data was the first irrefutable evidence for direct detection of a deeply buried hydrocarbon accumulation by subsea CSEM sounding. The technique has later shown very good results when applied correctly in the prospecting work flow. These results have opened a new frontier in hydrocarbon exploration.

In recent years different types of CSEM acquisition have evolved including horizontal dipole source with seabed nodes, horizontal dipole source with cable towed receivers, and vertical dipole source with seabed nodes. Here we will describe the seabed node receiver method using a horizontal towed dipole source.

The *marine* magnetotelluric method (MMT) is another offshore geophysical method measuring subsurface resistivity. This method is using the Earth's

K. Bjørlykke (ed.), *Petroleum Geoscience: From Sedimentary Environments to Rock Physics*,
DOI 10.1007/978-3-642-34132-8_20,

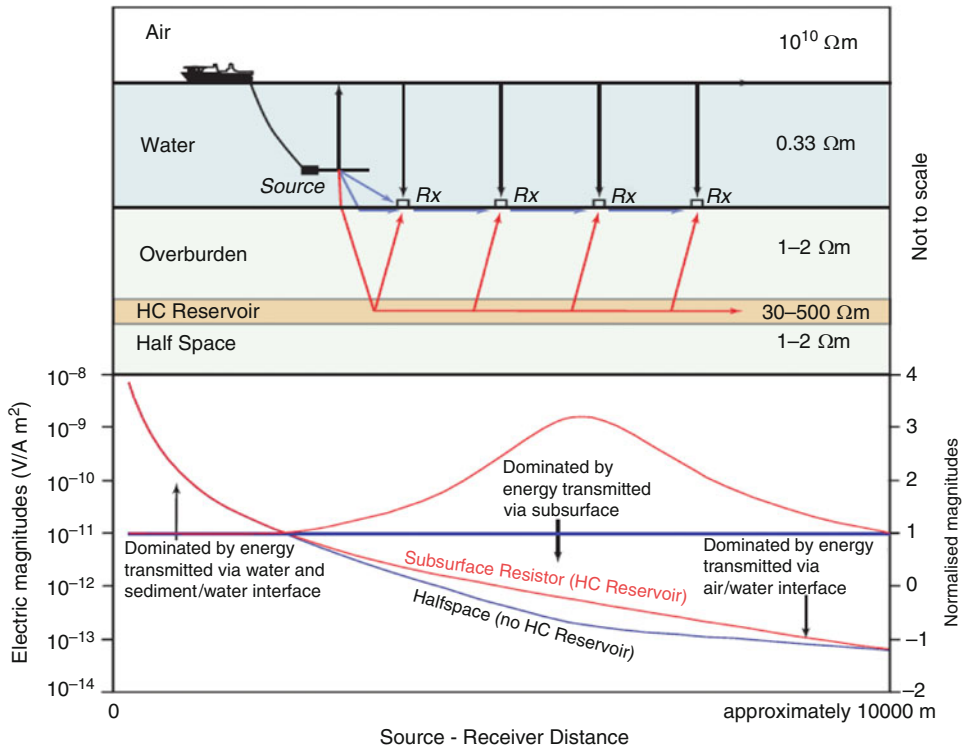

Fig. 20.1 (*Top*) Schematic sketch of air-water-sediment geometry and receiver (Rx) layout on seabed during towing of electromagnetic source. *Black arrows* denote refracted transmission of electromagnetic signals via the air/water interface. *Blue arrows* denote direct transmission of electromagnetic signals through water and by refraction along the seabed. *Red arrows* denote guided transmission of electromagnetic signals via a buried high-resistivity layer (hydrocarbon reservoir). (*Bottom*) Electric magnitudes measured at a single receiver as a function of source-receiver distance. *Red curve* shows the expected response from a model including a high-resistivity hydrocarbon reservoir. (*Lower curves*) *Blue curve* is the significantly weaker response from a model without a hydrocarbon reservoir. (*Upper curves*) To better visualise theoretical differences in amplitudes between the two cases the reservoir curve (*red*) was divided (normalised) by the no-reservoir curve (*blue*)

natural varying electromagnetic field as source. On *land* the method (MT) was introduced in the 1950s by the geophysicists Cagniard and Thikonov. MT can improve the interpretation of deep structures as it has very low frequency content, and it can image conductive sediments below thick resistors such as salt or basalt. For this reason the MMT application has created interest also in the hydrocarbon exploration industry.

20.2 CSEM Basic Concepts

20.2.1 Background

Resistivity variations in rocks are generally controlled by the interplay between highly resistive minerals and pore fluids including low resistive saline water and/or highly resistive hydrocarbons. Sedimentary rocks have a wide range of resistivities (0.2–1,000 Ωm) mainly controlled by variations in porosity, permeability and pore connectivity geometries in addition to pore fluid properties and temperature. It is the high resistivity of hydrocarbon filled reservoir rocks (30–500 Ωm) compared with reservoirs filled with saline formation water (0.5–2 Ωm) that makes EM sounding a good tool for detection of subsurface HC.

In marine CSEM sounding a horizontal electrical dipole is towed close to the seabed emitting a low frequency (0.1–20 Hz) signal which is recorded by stationary seabed receivers (Fig. 20.1). Seabed receivers record the EM responses as a combination of energy pathways including signal transmission directly through seawater, reflection and refraction via the seawater/air interface, refraction and reflection along the seabed, and reflection and refraction via possible high resistivity subsurface layers.

Low frequency EM signals decay exponentially with distance. The distance required to attenuate an

EM signal by the factor e^{-1} (appr. 0.37) is defined as the skin depth ($\approx 503\sqrt{\frac{\rho}{f}}$ [m]). It is about 551 m in seawater (0.3 Ωm) and 1423 m in 2 Ωm sediment and 10^8 m in air (10^{10} Ωm) for a 0.25 Hz signal. EM signals are rapidly attenuated in seawater and seafloor sediments saturated with saline water, and these signal pathways will dominate at near source-to-receiver offsets (~3 km). In high resistivity and relatively thin (20–200 m) subsurface media, such as hydrocarbon filled reservoirs (30–500 Ωm), the energy is guided along the layers and attenuated less depending on the property of the layer. Guided EM energy is constantly leaking back to the seafloor and is recorded by the EM receivers. Energy is also refracted along the air/water interface. This energy is commonly termed the air-wave and dominates at far offsets depending on water depth and the subsurface resistivity. The refracted energy from high resistivity subsurface layers will dominate over directly transmitted energy when the source-receiver distance is comparable to twice the depth to this layer. The detection of this guided and refracted energy is the basis of CSEM as used when exploring for thin HC layers.

20.2.2 CSEM Work Flow

Typical steps in a CSEM work flow are shown in Fig. 20.2, and in the following we focus on the steps most important for interpretation of CSEM data. The sensitivity study is a vital step before time and money is invested in a survey. Here it can be evaluated if targets are within reach of the selected EM method.

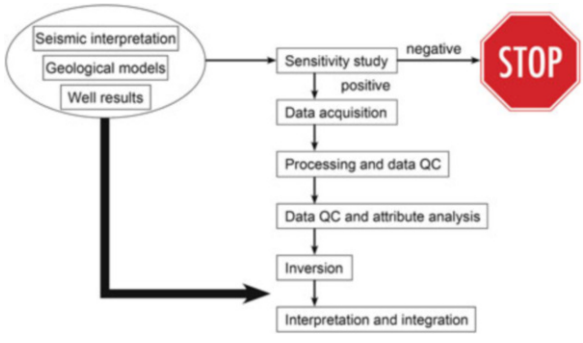

Fig. 20.2 CSEM work flow from sensitivity study to interpretation and data integration. Seismic data and existing geological knowledge is necessary to fully utilise the potential of the CSEM data

Forward modelling will give a good indication whether an EM survey will add new information or not. When data are acquired, adequate processing is critical for good data quality. To get the best result, the EM data must also be interpreted as early as possible in the processing work flow. Inversion is an integrated part of the interpretation work flow, and this is the best way to depth convert the EM data. When data are inverted it is also possible to integrate EM data with other geophysical and geological data.

20.2.3 Sensitivity Study and Survey Design

Prior to acquiring CSEM data a sensitivity study is performed. In this way we can find out if the defined target can be measured by the CSEM technique. A typical target is a hydrocarbon prospect. All available knowledge is gathered to build a representative Earth model. Resistivity both for the prospect and the background is included in the Earth model.

A prospect's sensitivity to the CSEM method can be analysed by forward modelling. In the modelling the expected CSEM response from the prospect is calculated. A prospect's sensitivity will depend on several factors such as: complexity of the background geology, prospect size, prospect geometry, prospect thickness, resistivity contrast between the prospect and background rocks, and burial depth for the prospect. Based on the results from the sensitivity study the actual survey design is decided.

Sensitivity to a target can be defined by several methods such as normalised magnitude (NMVO) response or phase difference response (PDVO). These attributes are created by dividing the target response by the background response (Fig. 20.1). The weakness of these measures is that they do not consider the whole field (i.e. they look at magnitude and phase separately) and they do not take the expected data uncertainty and noise into account. Figure 20.3 shows a better way to consider sensitivity which takes phase, magnitude, data uncertainty and background noise into account. The figure shows a 1D modelled magnitude and phase response at 1.0 Hz from a background model (blue curve) and a model including a reservoir (red curve). The green curve is the absolute field difference (magnitude and phase) of these two responses and represents the scattered field caused by the resistive reservoir. The purple curve is

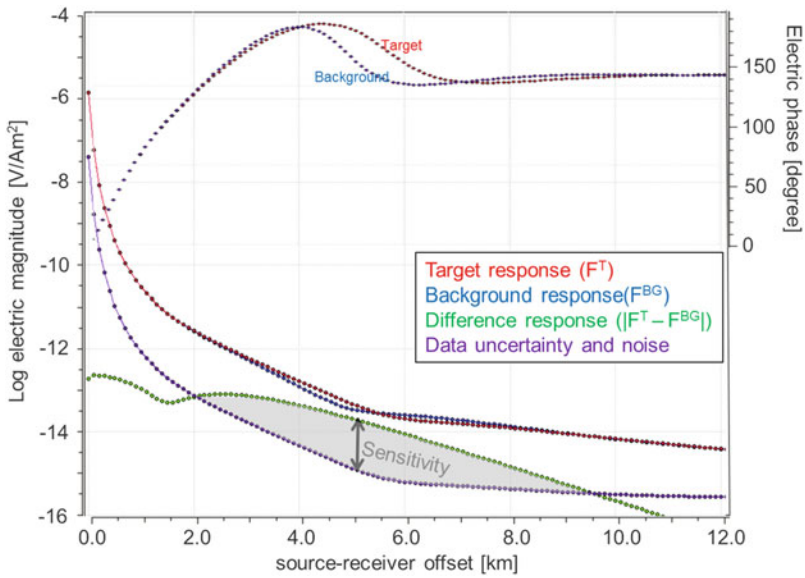

Fig. 20.3 Illustration on how sensitivity to a hydrocarbon reservoir can be calculated. Both magnitude and phase vs. source receiver offset responses are shown for a target (*red curve*) and background (*blue curve*). The difference response (*green curve*) represents the scattered field from the target only and is the absolute difference between the background and target response (both magnitude and phase included). The data is sensitive to the target only if the scattered field response is larger than the expected data uncertainty and noise (*purple curve*). See text for details

the assumed data uncertainty and noise when acquiring the data. This is taken from an experience data base. For short to intermediate offsets the acquisition measurement uncertainty will dominate the curve (scalable noise), and at long offset the background noise will dominate (additive noise). The latter is seen from 6.0 km offset where the noise curve flattens. From these curves we can define the sensitivity by dividing the scattered field response (green curve) by the expected data uncertainty and noise (purple curve). Hence a sensitivity <1 will have the scattered field response lower than the data uncertainty and noise (no sensitivity). This can be seen from offsets less than 2.0 km and offsets larger than 9.5 km. A sensitivity >1 is in the grey shaded area and means that the scatter field response from the target is higher than the expected data uncertainty and noise. This is where CSEM is sensitive to the target. Note that even though the magnitude difference between the target and background at 5.5 km source-receiver offset is zero, the grey sensitivity area is large. This is because the phase difference between the two scenarios at this offset is also large. Thus using the field response (magnitude and phase) gives a better sensitivity measure than using the phase and magnitude separately. The maximum sensitivity in this example is at approximate 5.0 km source-receiver offset, and is the *peak* sensitivity.

The left diagram in Fig. 20.4 shows a generalised workflow for the sensitivity study where all prior knowledge is used to build an Earth resistivity model for forward modelling. The results of the modelling will decide whether the project is seen as not feasible (project end) or feasible. In the latter case the work flow will continue with survey design and acquisition. Results from a sensitivity study are shown to the right in Fig. 20.4. On the vertical axis is the *peak* sensitivity as shown in Fig. 20.3. We have divided the peak sensitivity into three different zones: low, medium and high sensitivity (red, yellow and green zones). Low sensitivity is less than 1, and means that the target is not likely to be detected. Medium sensitivity is between 1 and 3, and means that the target could be detected. High sensitivity is larger than 3, and means that the target is very likely to be detected. Along the horizontal axis the transverse resistance is plotted. Transverse resistance is the product of the net pay thickness of the target and the resistivity of the target. For example, a transverse resistance of 2,000 Ωm^2 could be a target with 50 m net pay and target

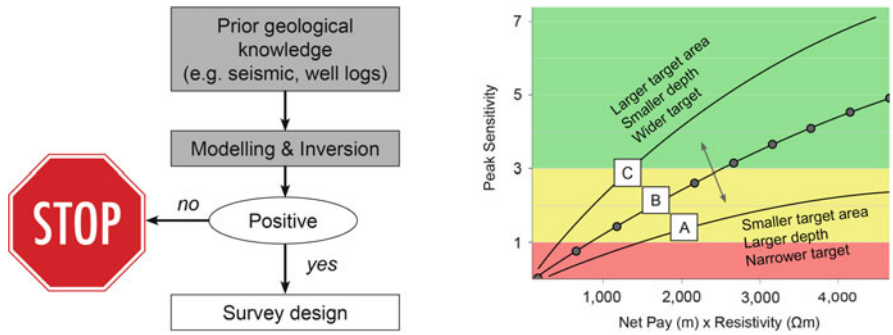

Fig. 20.4 CSEM sensitivity study procedure (*left*) and target sensitivity diagram (*right*). A, B and C show sensitivity for three different targets as a function of transverse resistance (target net pay thickness and resistivity contrast). The curve describing target B is the sensitivity to a given target with a burial depth of 1,500 m below mudline. The curve describing target A has an identical target size and geometry as B, but a burial depth of 2,000 m below mudline. The curve describing target C has the same target burial depth as B, but with a larger target area. *Red area* is regarded as low sensitivity (<1), *yellow area* is medium sensitivity (1–3) and *green area* is high CSEM sensitivity

resistivity contrast of 40 Ωm, or a target net pay thickness of 40 m and a resistivity contrast of 50 Ωm. These two scenarios will give approximately equal CSEM response if the burial depths are comparable. The transverse resistance is one of the main parameters that control the CSEM sensitivity.

To demonstrate the effect of burial depth, target size and target form, three examples are included in Fig. 20.4. Peak sensitivity for the three targets (A, B and C) with increasing transverse resistance is plotted in the diagram. The curve describing target B is the sensitivity to a given target with a burial depth of 1,500 m below mudline. The curve describing target A has an identical target size and geometry as B, but a burial depth of 2,000 m below mudline. The curve describing target C has the same target burial depth as B, but with a larger target area. If we follow the curve of target B we can see that this target is not likely to be detected by CSEM if the transverse resistance is less than 900 Ωm^2 (e.g. 18 m net pay and 50 Ωm reservoir resistivity), but is very likely to be detected if the transverse resistance is larger than 2,500 Ωm^2 (e.g. 50 m net pay and 50 Ωm reservoir resistivity). The difference between the curves A, B and C shows how the sensitivity will vary as a function of target area, shape and burial depth. For a given transverse resistance value the sensitivity will increase with for example decreasing burial depth and/or increasing target area. For example at a transverse resistance of 1,500 Ωm^2 (e.g. 30 m net pay and 50 Ωm reservoir resistivity) target A is not likely to be detected, target B could be detected and target C is very likely to be detected.

In addition to forward modelling studies providing CSEM sensitivity to a target, a sensitivity study can also include inversion of the synthetic data. An extended sensitivity study is typically done when the initial sensitivity results are in the moderate zone (yellow). Based on a detailed sensitivity study, acquisition parameters such as frequency bandwidth and receiver-source configuration can be selected. It is also worth noting that a sensitivity study is not, of course, the absolute truth. The selected parameters can still be uncertain. Therefore as a part of a complete sensitivity study, the study itself should be evaluated, and the results risked before they are used in the evaluation.

20.2.4 Data Acquisition and Processing

Both 2D and 3D CSEM acquisition can be performed. In early 2000, when the CSEM method was established in HC exploration, only 2D data was acquired. However, since 2008 3D acquisition has been the preferred way to acquire CSEM data. It provides better data coverage, and gives an improved image of the subsurface. Today 2D acquisition is typically performed to tie CSEM survey lines to nearby wells and discoveries, or as long regional lines for structural imaging.

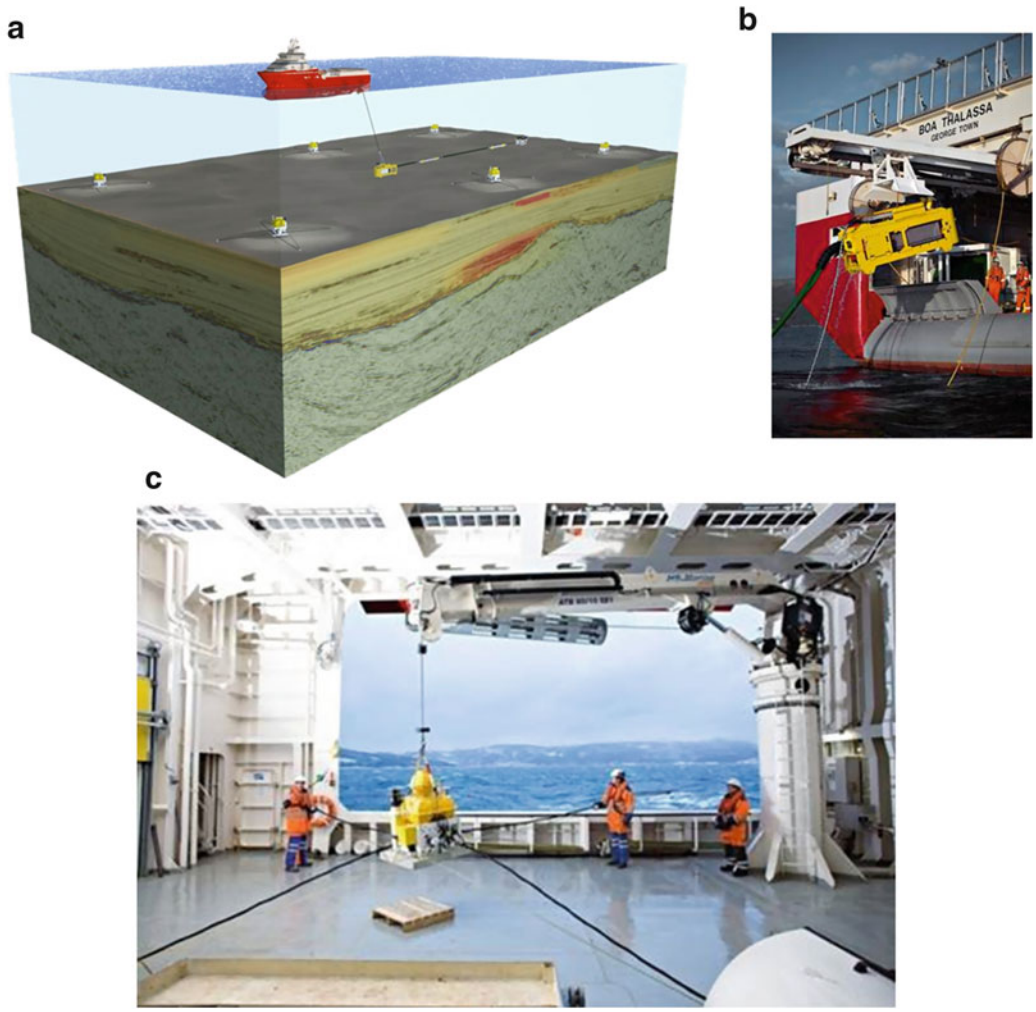

Fig. 20.5 (**a**) 3D CSEM acquisition with a receiver grid layout and a dipole source. (**b**) Deployment of the source. (**c**) Deployment of the receivers

When acquiring 3D marine CSEM data, receivers are placed on the seabed in a grid covering the area of interest. The source is towed above the receiver grid in a predefined pattern (towlines) while all receivers on the seabed are recording (Fig. 20.5a). A 2D CSEM acquisition has receivers placed only along one receiver line and the source is towed directly above these receivers. Hence, there are no receivers off the actual source towline.

The receivers consist of electric antennas and magnetic coils typically measuring in two horizontal perpendicular directions (Fig. 20.5c). They are placed on the seabed simply by letting them sink freely down to pre-planned positions. The orientation of the receiver antennas will therefore be in random directions for each receiver.

When all the receivers are placed on the seabed the CSEM source is deployed (Fig. 20.5b) and towed above the receivers. The source is an electric dipole emitting an electromagnetic field. The horizontal electric dipole antenna consists of two electrodes separated from each other, and with electrical contact to the seawater. The source transmits a continuous and designed signal with a low fundamental frequency. The frequency range spans from 0.1 to 20 Hz, with the main energy output at the lower part of the spectrum. The peak current can vary from 1,000 to 8,000 a, depending on the actual design of the transmitter.

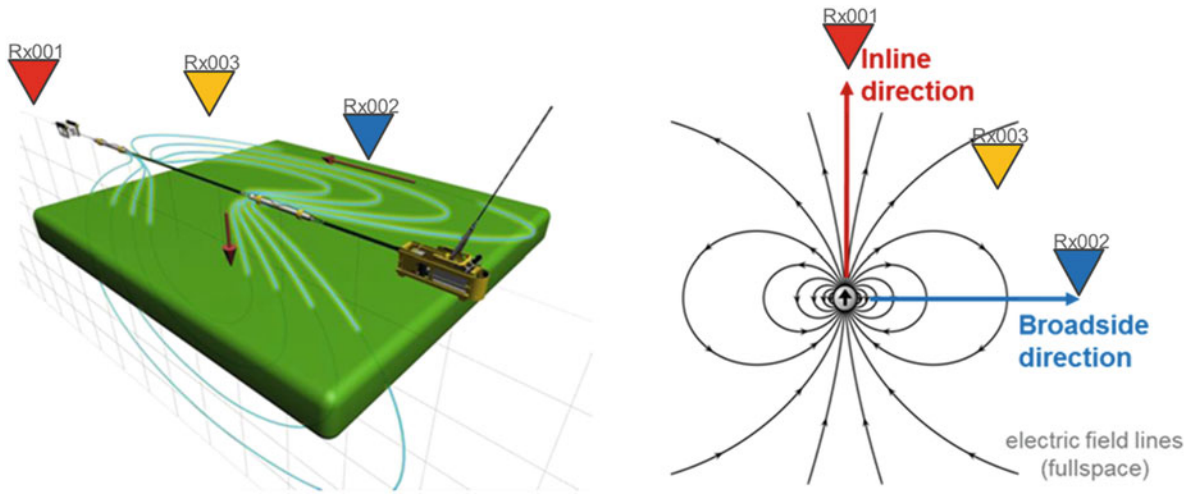

Fig. 20.6 Types of antenna configuration and EM fields. When the source- and receiver antennas are in line with each other the configuration is called inline. When the antennas are parallel and perpendicular to each other the antenna configuration is called broadside. Receivers Rx001 and Rx002 are placed in an inline and broadside position respectively. Receiver Rx003 is located at a position acquiring azimuthal data. This receiver will measure both inline and broadside data. A 2D survey with receivers only along the source direction (Rx001) will only record inline data

During a 3D acquisition the source antenna and receiver antenna will form varying configurations. When the source- and receiver antennas are in line with each other the configuration is called inline and the data collected are inline data. When the antennas are parallel and perpendicular to each other the antenna configuration is called broadside and the collected data are broadside data. In Fig. 20.6 the two antenna configurations (inline and broadside) are shown. The position of receivers Rx001 and Rx002, with respect to the source position, are placed at an inline and broadside position respectively. Most of the antenna configuration within a 3D CSEM survey will be antenna configuration with an azimuth component. Such data is called azimuthal data. Receivers Rx002 and Rx003 are located in a position acquiring azimuthal data, and will measure both inline and broadside data.

The Earth is anisotropic and has different resistivity properties in the vertical and in the horizontal direction. The inline antenna configuration is mainly sensitive to the vertical resistivity, while the broadside configuration is mainly sensitive to the horizontal resistivity of the Earth. This is one of the reasons why 3D data acquisition is superior to 2D acquisition.

After data acquisition the receivers are released from the seabed and data can be downloaded for processing (Fig. 20.7). The recorded time series on each receiver are calibrated and transformed to the frequency domain using Fourier transform. The pre-conditioning step involves dipole antenna scaling and stacking of dual channels on the receivers. The antennas of the receivers are oriented randomly because receivers are sinking freely down to the seabed. When using the receiver data for quality control and attribute analysis, inline and broadside components are calculated for all receivers. This is done through a processing step where receivers are mathematically rotated, and receiver antennas become either inline or broadside oriented. An example of rotated receiver data at 0.25 Hz frequency is given in Fig. 20.8. The receiver data is plotted as magnitude vs. source-receiver offset (MVO) and phase vs. source-receiver offset (PVO). These data are used as input for attribute analysis and for inversion algorithms to produce Earth resistivity models.

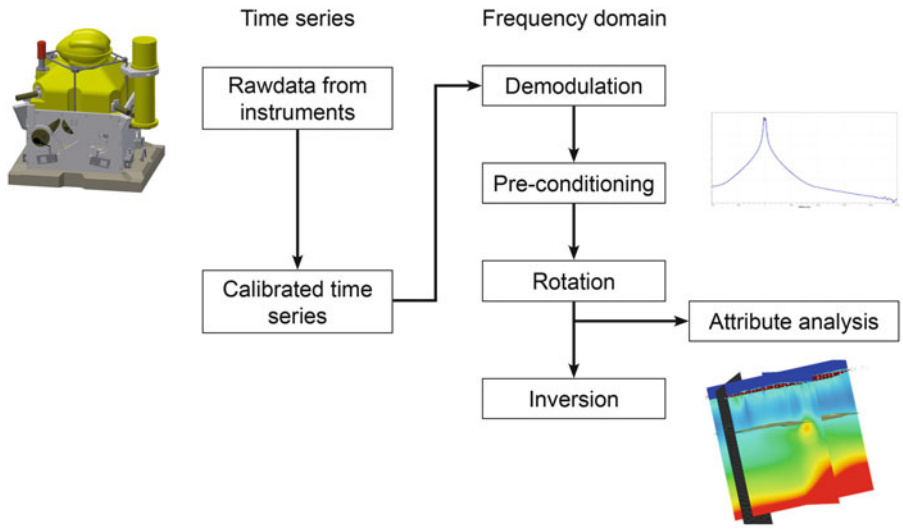

Fig. 20.7 Simplified CSEM processing workflow from receiver data download to 3D resistivity cube. The recorded time series on each receiver are downloaded and calibrated. Each receiver is transformed from the time domain to the frequency domain (demodulation). Pre-conditioning involves receiver channel summation and scaling of the source dipole moment. Before attribute analysis and inversion the receiver data is mathematically rotated into inline and broadside components

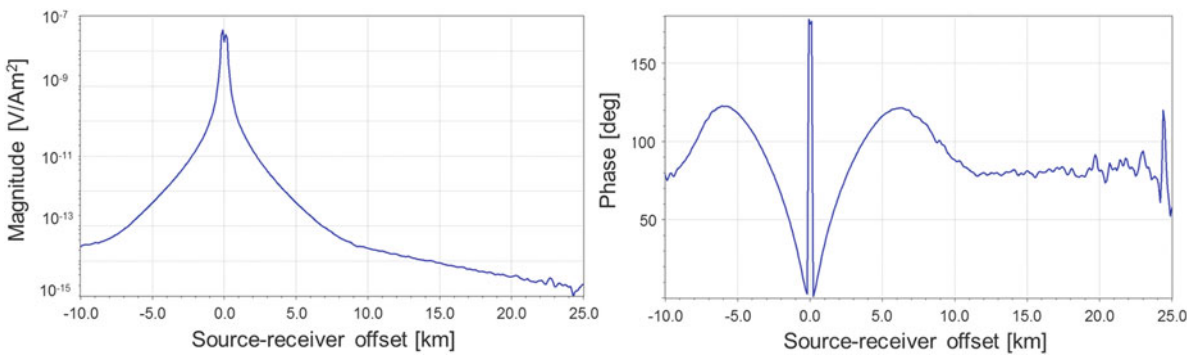

Fig. 20.8 Magnitude vs. offset (MVO) to the left and phase vs. offset (PVO) to the right for one receiver at frequency 0.25 Hz. Along the x-axis is the source-receiver offset where offset 0.0 is the location of the receiver. Negative offsets are called in-tow and describe offsets when the source is approaching the receiver. Positive offsets are called out-tow and describe offset when the source is moving away from the receiver. Also compare with Fig. 20.1

20.2.5 Inversion

When we do electromagnetic acquisition (CSEM and MT) the goal is to find the resistivity distribution in the subsurface. However, what we measure is the electric and magnetic fields recorded at the seabed. This is a typical inverse problem as we seek a parameter (the resistivity of the Earth) which we cannot directly measure. In general terms an inversion problem can be solved by finding the model m which explains the measured data d using an operator G. The operator G describes the explicit relationship between the model (m) and the observed data (d):

$$m = G^{-1}(d)$$

For the CSEM and MT methods the model m is the Earth resistivity distribution that we are seeking and d is the electric and magnetic field measured by the receivers. However, we have several problems with this equation. First of all we do not know the inverse operator G^{-1}. Second the operator G, which is forward modelling based on Maxwell equations, is nonlinear. Third the solution to our problem is ill posed. To understand what ill posed means lets define a well posed problem. A well posed problem means that a solution exists. There is a unique solution (same data measurement can only be explained by one model), and the solution is stable (a small change in the model creates a small change in the data measurement). If one or more of these terms are broken we have an ill posed problem. For CSEM and MT data our largest challenge is the non-uniqueness. This means that several resistivity models can create the same data measurements. We can also be challenged with an unstable solution. Because of the complexity of our problem, we must do approximations and find the solution in an iterative way. Instead of finding the Earth resistivity model by using the inverse operator G^{-1} (which is unknown), we perform forward modelling to simulate synthetic data based on a given model:

$$d = G(m)$$

The final inverted resistivity model is obtained by finding a model, m, which gives the minimum difference between the synthetic data, d, and the measured data using e.g. least square methods. These inversion results will depend on the start model used, the regularisation terms, a priori information applied to constrain the results, and the number of dimensions used in the forward modelling algorithm, G (1D, 2D or 3D). Due to the non-uniqueness of the solution, performing inversion is just as much an interpretation task as a data processing step.

Figure 20.9 shows a schematic diagram of how this type of inversion works. Inversion of electromagnetic data starts by making a qualified guess of an initial Earth resistivity model. This is the start model, m^0. The start model can be similar to the background model used in the sensitivity study, or an updated model using new information from real data analysis and lower dimension inversion results. Forward modelling is performed on the start model using receiver- and source geometry which is identical to the real data acquisition configuration. The forward modelled data, d, are compared with the measured data. The difference between these two data sets

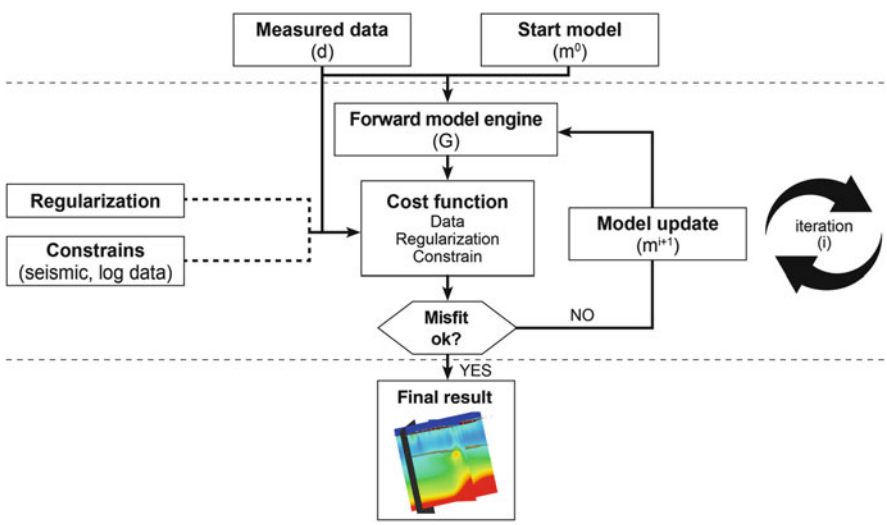

Fig. 20.9 Flowchart for inversion. See text for details

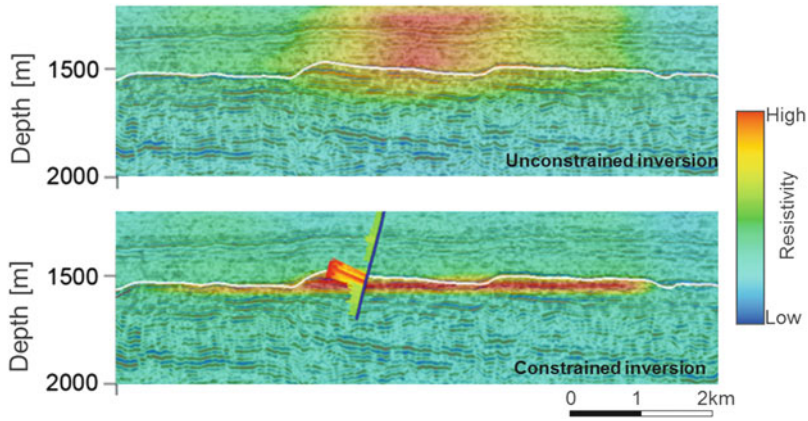

Fig. 20.10 Unconstrained (*upper*) and constrained (*lower*) 3D CSEM inversion results are overlain depth migrated seismic data and well data (blue line). The example is from the Western Troll oil province in the North Sea, offshore Norway. The improved resolution of the reservoir is clearly seen in the constrained inversion result. Note that this example is based on a very good understanding of the background resistivity. This knowledge is used in the start model for the constrained inversion. The constraints favour resistivity model updates within the reservoir level defined by seismic horizons. Data courtesy EMGS

gives the data cost which expresses how well the start model explains the measured data (misfit).

Because the inversion solution is non-unique it may be necessary to introduce regularisation. In the regularisation process additional information is added to solve the ill-posed problem. In our case regularization terms could for example be to seek a smooth horizontal layered resistivity model. The data- and regularisation cost adds up to the total cost function, Φ:

$$\Phi = \text{Data cost} + \text{Regularisation cost}$$

The goal of the inversion is to update the resistivity model in such a way that the total cost function is minimised. One loop within the flowchart involves forward modeling of a model and calculation of the cost function. If the cost function (or misfit) is unacceptable the inversion performs new updates of the resistivity model (m^{i+1}) and starts a new loop. A complete loop is called one iteration within the inversion. The inversion iterates until the total misfit goes below a certain value, or is stopped by the user when it converges towards one value with respect to iteration number.

An inversion process that only uses the electromagnetic data itself and no other input is called an unconstrained inversion. A further step in the inversion process is to apply constraints to the model based on other geological or geophysical data. Constraints can be regarded as restrictions to the inversion solution in order to comply with these data. They will therefore limit the solution space and force the inversion towards a particular solution. Examples of constraints can be that the inversion is only allowed to update the model within a certain layer defined by seismic horizons (Fig. 20.10), or that the updates within a layer should be within a resistivity interval taken from well log data. Constrained inversion will usually give an Earth model with improved resolution. However, it is important to note that the restrictions put on the model update can also lead to a wrong result. If the assumptions used in the constraints are wrong, the solution will also be wrong. Constrained inversion is therefore usually performed in areas where one has good prior knowledge, and it is recommended that an unconstrained inversion is always performed for comparison.

The final output from an unconstrained or constrained inversion is an Earth resistivity model. This model is only one of several possible solutions which fit the measured data, and the final results should be carefully evaluated. First, the entire data misfit, or how well the synthetic data from the model describes the measured data, should be inspected. Has the total misfit from the inversion converged with increasing iterations? Are there areas where the misfit is too large? Second, the final resistivity model needs to be evaluated with respect to the general geological

model. Do the resistivity variations follow the expected trends? How well do resistivity anomalies fit with the anticipated results? If the results are not as expected, it does not necessarily mean that the inversion results are wrong. It can just as well be that the existing geomodel is wrong and needs to be redefined. It is within this integrated interpretation process between electromagnetic-, seismic- and well-data that valuable additional information can be extracted.

20.2.6 Interpretation and Integration of CSEM Results

Interpretation of CSEM data involves explaining the resistivity changes that we observe from real CSEM data, and relating these to lithology and fluid changes in the subsurface. The interpretation needs to be integrated with other geophysical and geological data to build a geological model that honours all the available data.

When interpreting CSEM data it is important to keep in mind that the ability to detect hydrocarbon reservoirs is not only dependent on the resistivity contrast between the reservoir and the surroundings, but also on burial depth, target size and net pay thickness of the reservoir. Furthermore the acquisition geometry will also be of importance. A dense receiver grid will be able to detect smaller targets than a coarse receiver grid. The presence of a resistor could indicate a hydrocarbon reservoir, but could also be explained by other resistivity anomalies. It could for example be caused by low porosity rocks (e.g. cemented or tightly compacted sandstones), highly organic-rich shale (source rocks), carbonates, volcanic rocks, salt or other high resistivity strata or structures in the subsurface. Further, integration of seismic data, well logs and geological understanding will help to reduce the possible explanations of an observed resistivity anomaly.

Interpretation of CSEM data can be done at a very early stage in the processing flow by analyzing relative differences between receivers. This can for example be done on normalised magnitude vs. offset (NMVO) displays, or phase difference vs. offset plots (PDVO). An increase in NMVO indicates a resistivity increase in the subsurface relative to the reference receiver used for the normalisation (Fig. 20.1). Similarly a decrease in PDVO (Fig. 20.3) will indicate a resistivity decrease in the subsurface. Such interpretations will give a first indication of resistivity changes in the subsurface. It will mainly provide information about lateral resistivity changes, but can also give rough estimates of burial depth to a resistor. A deeply buried resistor will show up at larger source-receiver offsets and lower frequencies than a shallow resistor. As a rule of thumb the burial depth to a resistor can be approximated to half the source-receiver offset at the onset of the anomaly. This approximation assumes a 1D Earth. Interpretation of receiver data attributes (such as NMVO and PDVO) is important as it directly evaluates the recorded data. The Troll case is included as an example of receiver interpretation. In the other cases the interpretation is based on inversion results.

Inverted resistivity models can be directly integrated with depth converted seismic and well log data. When interpreting CSEM inversion results it is useful to look at vertical depth sections as well as resistivity maps. Depth windows for resistivity maps can be selected by constant depth intervals, or to follow seismic depth converted horizons. Such maps give the lateral outline of resistive anomalies which can be correlated with seismically defined structures.

It is also important to quality control and interpret the CSEM data at different processing levels from attributes in the receiver domain to full 3D inversion. Figure 20.11 shows an example where a resistor is consistent at different processing steps. A significant normalised magnitude anomaly (purple shadow) is clearly visible early in the processing (receiver level, upper left picture). In this image the source-receiver offset is plotted along the vertical axis. The burial depth to the resistor can be approximated to 1.5 km which is half the source-receiver offset of the anomaly onset. The same anomaly also stands out in the 2.5D inversion result along the line (middle left picture). The burial depth and lateral extent agree with the initial interpretation of the NMVO attribute. The lower left picture shows the 3D inversion result along the same acquisition line and the areal extent of the anomaly is shown in map view in the upper right picture in Fig. 20.11. The anomaly also conforms to a faulted structure when overlain seismic data (lower right picture). In this case the analyses done on the CSEM data at different processing levels are consistent, and indicate a subsurface resistor with significant contrast to the surroundings. However, the detailed nature of the resistor can only be understood by using all available geophysical and geological knowledge in the area.

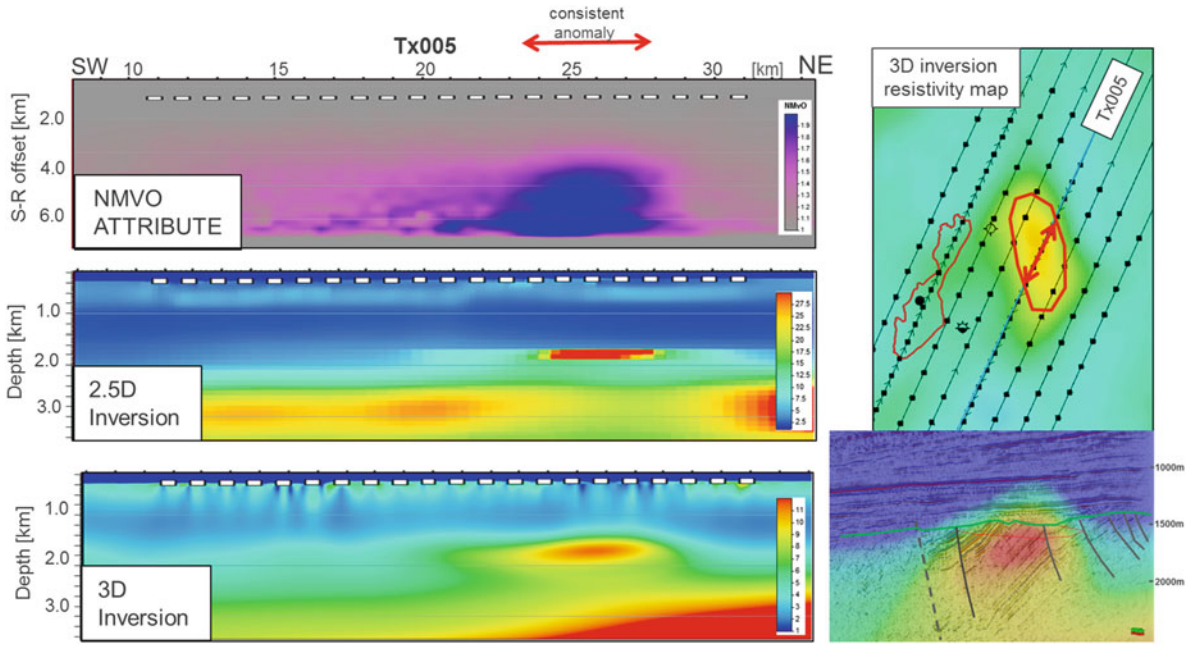

Fig. 20.11 Real data example from the Norwegian Sea showing a resistive anomaly which is consistently identified from normalised magnitude vs. offset attribute (*Upper left*) through 2.5D inversion (*middle left*) and 3D inversion (*lower left*). The map outline of the anomaly also correlates at depth with a faulted structure (*right*). Data courtesy EMGS

20.2.6.1 Electrical Anisotropy

Sediments and layered strata can be strongly electrically anisotropic. This is a combination of intrinsic anisotropy (e.g. anisotropy within the shale) and large-scale anisotropy (e.g. anisotropy due to thin bed layering). If anisotropy is not taken into account it can easily lead to false inversion- and interpretation results. Most forward modelling and inversion algorithms assume a TIV media (Transverse Isotropic with a Vertical axis of symmetry). This means that electrical properties of subsurface rocks are described by a horizontal and a vertical resistivity component. The anisotropy is defined as the vertical divided by the horizontal resistivity component. Typically, vertical resistivity will often be higher than horizontal resistivity due to the horizontal layering of beds and strata. Today most resistivity well log tools only measure the horizontal resistivity. In such cases it is only possible to directly calibrate the horizontal resistivity model to the well logs.

When tri-axial resistivity logging tools measuring both directions become more common, calibration also of the vertical resistivity model derived from CSEM data will be possible. Better understanding of the electrical anisotropy will improve our ability to interpret CSEM data.

20.2.6.2 Apparent Anisotropy

As explained above, 3D CSEM acquisition provides both inline- and broadside data. The inline data is sensitive to the vertical resistivity (Rv) in the Earth, while the broadside data is sensitive to the horizontal resistivity (Rh) in the subsurface. Azimuthal data measures both inline and broadside data, and is therefore sensitive to both horizontal and vertical resistivity.

In addition it is only the in-line data that is sensitive to thin horizontal resistive layers. The broadside data is not able to detect thin horizontal resistive layers, but measures background resistivity trends. This is because horizontal currents will flow around a thin resistor while vertical currents will not. The situation is opposite for thin vertical resistors. Here vertical currents can flow around the resistor while horizontal current will not. In this case the vertical resistor will be imaged better in the horizontal resistivity model than in the vertical resistivity model.

The difference in sensitivity can be illustrated by using a synthetic example (Fig. 20.12). The upper panels show the Earth model's vertical (left column) and horizontal resistivity (right column). The thin resistor (red target) is a hydrocarbon reservoir with equally high vertical and horizontal resistivity.

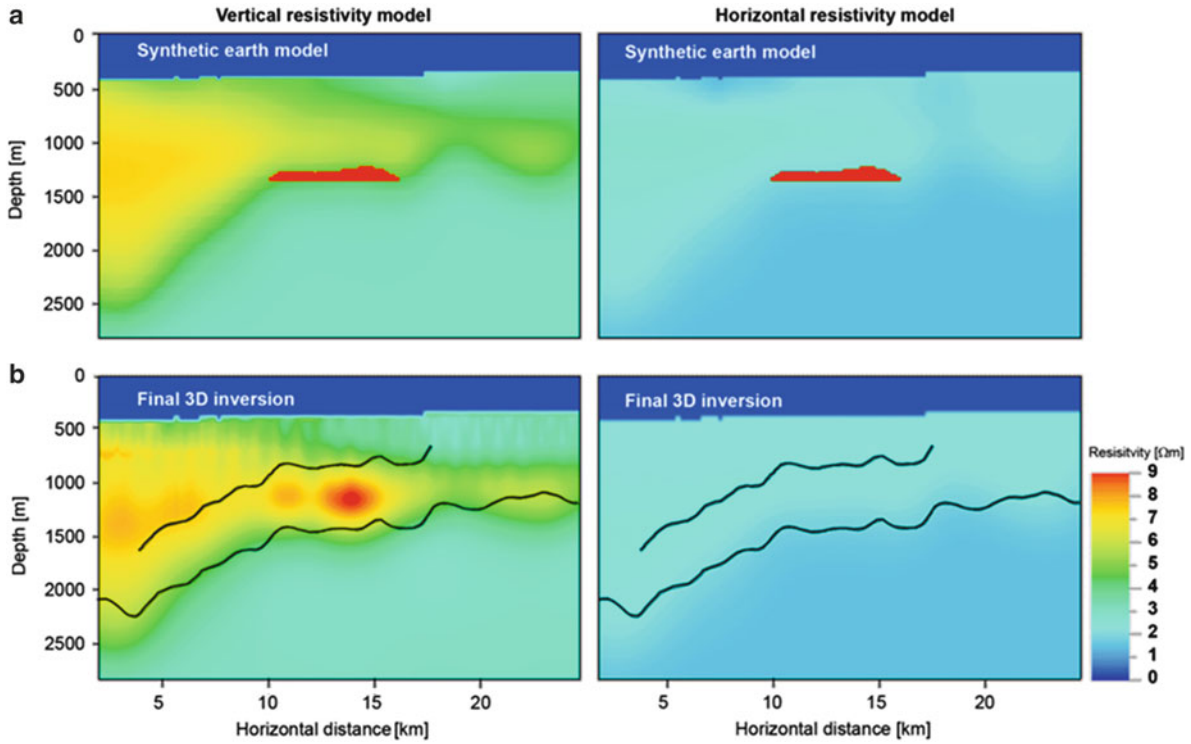

Fig. 20.12 Unconstrained 3D inversion of synthetic CSEM data. (**a**) The resistivity model used for forward modelling, vertical resistivity model, R_v, (*left*) and horizontal resistivity model, R_h, (*right*). The inverted resistivity result is shown in (**b**). Due to difference in sensitivity only the inverted R_v model images the thin target, the inverted horizontal resistivity model images the background resistivity. See text for a more detailed explanation

Hence, the anisotropy in the thin hydrocarbon layer is equal to one. Based on this Earth resistivity model, synthetic 3D CSEM data are simulated, and unconstrained 3D inversion is performed on the synthetic data. The inversion result for both the vertical and horizontal resistivity models is shown in the lower panel in Fig. 20.12. The results confirm that the CSEM method is not sensitive to the horizontal resistivity within the thin layer. It is only the inverted vertical resistivity model that reconstructs a resistive anomaly at reservoir level. The inverted horizontal resistivity model does not reconstruct the thin reservoir, but provides an image of the background resistivity.

For these reasons, thin resistors will show high electrical anisotropy (R_v/R_h). We call this *apparent anisotropy* as it is not the "true" anisotropy in the thin layer, but rather an effect of the difference in sensitivity between inline- and broadside data. Therefor, for thin resistors the horizontal resistivity of the layer is not measured, only the background horizontal resistivity is detected. Apparent anisotropy can be used as an interpretation attribute for better separating thin resistors, possibly associated with hydrocarbon reservoirs, from thicker resistors associated with background variations. Both thin and thick resistors will show up as resistive anomalies in the vertical resistivity model, but only the former will also have an apparent anisotropy anomaly.

20.3 Marine Magnetotelluric: Basic Concepts

20.3.1 Background

Marine magnetotelluric (MMT) is an offshore geophysical method measuring the Earth's resistivity using the Earth's natural varying electromagnetic field as source. Magnetotelluric (MT) on land has

existed for many years, but it is only in the last decade it has been widely used offshore. While CSEM is used primarily for detection of relatively shallow and thin horizontal resistors such as hydrocarbon reservoirs, MMT can only image larger-scale structures. It can improve the interpretation of deep structures, and due to the very low frequency content the energy can penetrate several tens of kilometres into the subsurface. More importantly it can image conductive strata below thick resistors such as salt or basalt. Because of this, MMT application has also created interest in the hydrocarbon exploration industry. Presence of salt or basalt in a basin often complicates seismic imaging, and MMT's ability to see through such layers has shown to be very valuable.

The naturally varying electromagnetic field is set up by two external sources. The low frequency content (<1 Hz) is caused by solar winds (stream of protons and electrons) interacting with the Earth's magnetosphere, while the high frequency content (>1 Hz) is worldwide lightning, mostly around the equator, which charges the Earth's ionosphere. These complex processes create a plane electromagnetic field travelling vertically downward through the atmosphere. Most of the energy is reflected back again when it hits the Earth surface, but part of the signal penetrates into the subsurface. This field induces currents in the Earth called *telluric currents* which again set up a secondary magnetic field. The strength of the secondary field is dependent on the electrical properties in the Earth. Measuring this signal will therefore provide information about subsurface resistivity. In marine magnetotelluric it is the low frequency signal set up by the interaction between the solar wind and the magnetosphere that will dominate. The conductive seawater will filter out all frequencies above approximately 1 Hz. The signal strength also varies with latitude. Areas close to the poles have stronger source signals than areas close to the equator.

20.3.2 Acquisition of MMT Data

An MMT survey is acquired by placing receivers on the seabed. The MMT signal is extremely weak, so high sensitivity receivers, recording both the electric and magnetic fields, are needed. Receivers can be placed as a single line, or in a receiver grid with typical receiver spacing of 1–5 km. Often a MMT survey is done in combination with CSEM acquisition. However, due to the low frequency signal it is important that enough listening time, undisturbed by the controlled source, is allowed when planning a survey. Typically it is necessary to listen for several days in order to get enough samples to describ the low frequency signal (Fig. 20.13). Required listening time will also vary with latitude. Close to the equator the signal is weaker, and longer listening time is needed to maximise the number of periods describing the low frequency signal.

MMT surveys in areas with large water depth will only obtain the lower frequency signals. This filtering of the high frequencies has implications for the imaging capabilities and will result in reduced resolution in the shallowest part of the section.

20.3.3 Basic Interpretation of MMT Data

The Earth resistivity can be described by impedance tensors. These tensors can be found by analysing the relationship between the recorded E and H fields (electric and magnetic). The processed receiver data results in apparent resistivity and impedance phase as a function of the signal period (T). In Fig. 20.14 the TE- and TM modes are plotted as a function of period. The transverse electric mode (TE) is the electrical polarised mode where the electric field is in the geological strike direction. The transverse magnetic mode (TM) is the magnetic polarised mode where the magnetic field is in the geological strike direction.

The apparent resistivity plot can be directly interpreted as it gives the resistivity average of the subsurface. The time period can roughly be transferred to minimum approximate burial depth by using the skin depth ($\delta \sim 500\sqrt{\rho T}$). For example a signal period (T) of 10 s with apparent resistivity (ρ) of 1.5 Ωm in Fig. 20.14 (upper) corresponds to a minimum burial depth of 2.0 km. The two different modes start to separate at a signal period of 100 s (Fig. 20.14, lower), indicating that there is a deeply buried three dimensional structure at minimum 7 km depth. Displaying the apparent resistivity or impedance phase for a complete receiver line with the signal period along the y-axis, and the different receiver responses along the x-axis can therefore provide a

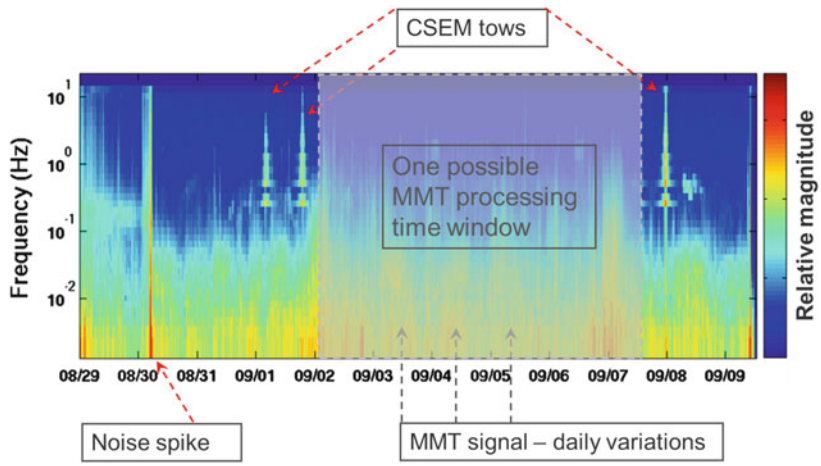

Fig. 20.13 Receiver recording as a function of time (days along x-axis) and frequency (y-axis). Both the controlled source signal (Christmas trees) and the time-varying MMT signal are visible in the plot. Note that the strongest MMT signal is recorded during day time. The *grey square* indicates a time window which can be used for MMT processing. This window is not influenced by the controlled source acquisition

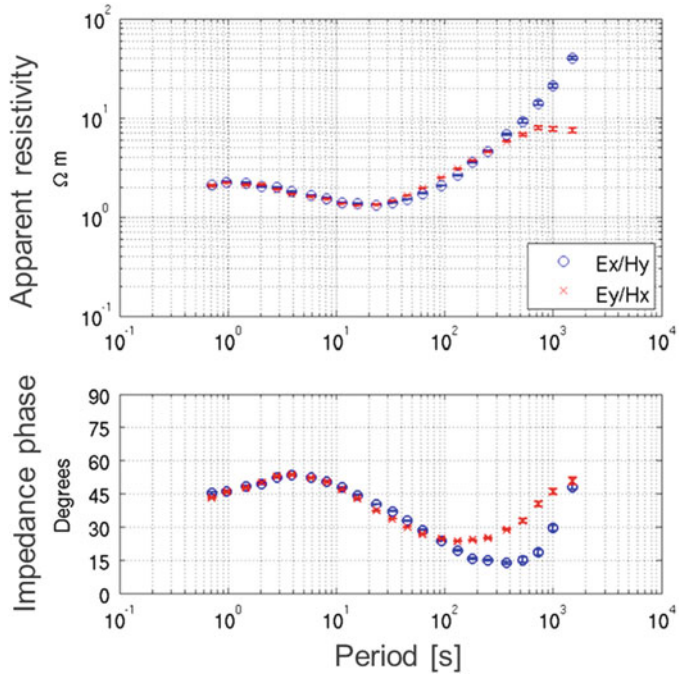

Fig. 20.14 Apparent resistivity (*upper*) and impedance phase (*lower*) processed from a recorded electromagnetic signal. *Blue circles* are the TE mode and *red crosses* are the TM mode. The transverse electric mode (TE) is the electrical polarised mode where the electric field is in the geological strike direction. The transverse magnetic mode (TM) is the magnetic polarised mode where the magnetic field is in the geological strike direction. The separation of the two modes with increasing period (decreasing frequency) suggests that there is a 3D structure at large burial depth

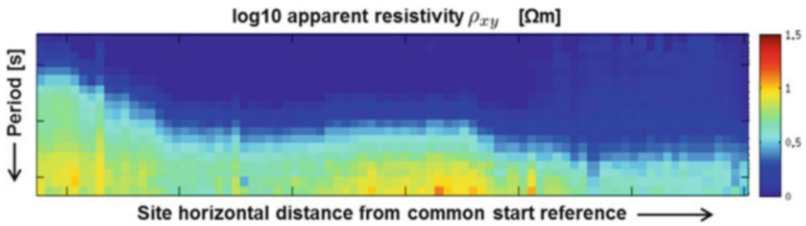

Fig. 20.15 Apparent resistivity display for the TE mode where lateral distance is along the x-axis and signal period (~depth) is along the y-axis. Such displays can quickly give an idea of the dominant structures in the subsurface. Here the transition from *blue* to *yellow colours* indicates the depth to a significant change in resistivity. This could for example be interpreted to represent the basement of a sedimentary basin. Stand-alone interpretation of MMT data can be difficult, and integration with other geological or geophysical data is important

good indication of the main subsurface structures (Fig. 20.15).

The apparent resistivity and impedance phase data is used as input to inversion. The inversion transforms the recorded data to a depth converted resistivity model (see inversion section for details). MMT inversion algorithms only invert for the horizontal resistivity model as the natural source is dominantly a plane horizontal field. The polarisation of the field is also why the MMT method will see through horizontal resistors such as basaltic layers. MMT data is used in combination with CSEM data to map structures beneath basaltic layers. MMT data can also be effective in mapping subsurface salt structures.

20.4 Troll Case Study

20.4.1 Troll West Gas Province

In this case study we present CSEM data across the Troll West Gas Province (TWGP), offshore Norway. The case is included as an example of pre-inversion interpretation of marine CSEM data at receiver level.

The Troll Field complex is the largest gas discovery on the Norwegian Continental Shelf, located in 300–360 m of water in the northeastern part of the North Sea. The field is subdivided into three separate compartments. Troll East is by far the largest and contains two thirds of the HC reserves. For the CSEM survey the much smaller TWGP was selected (Fig. 20.16). The reservoir interval is Jurassic sandstones (Sognefjord Fm.) with up to 160 m gas column, and a thin oil leg at the base. HC-filled sands show high average resistivities around 200–500 Ωm, and occur at a burial depth of about 1,400 m below sea level. Water-bearing Sognefjord Fm. sands and overburden sediments show resistivities in the 0.5–2 Ωm range. The TWGP was very well suited for CSEM surveying, due to the high reservoir resistivities, well defined field edges, the low and relatively constant resistivities in the geological layers above the reservoir (overburden), constant water depth, smooth seafloor, and the moderate distribution of the HC filled reservoir.

20.4.2 CSEM Forward Modelling

When interpreting CSEM data at receiver level the CSEM response over the HC accumulation is compared with the CSEM response in a reference area immediately outside the accumulation. It is also critical to understand CSEM responses from high resistivity bodies, other than the HC reservoir itself, which can potentially generate significant responses.

Three dimensional modelling shows how the CSEM response is affected by the geometry of the reservoir and the effect of varying receiver layout geometries. With the ultra-low frequencies (0.25 Hz) used in CSEM sounding, it is the resistivity variations in the illuminated subsurface that dominate the response measured at the seafloor. All measured and modelled CSEM responses are normalised to a reference case with no subsurface HC accumulation.

In this early case study, modelling had two main goals; firstly, to establish the optimal survey location and receiver geometry; and secondly, to quantify the expected CSEM response from the subsurface HC accumulation relative to that of a reference area outside the accumulation.

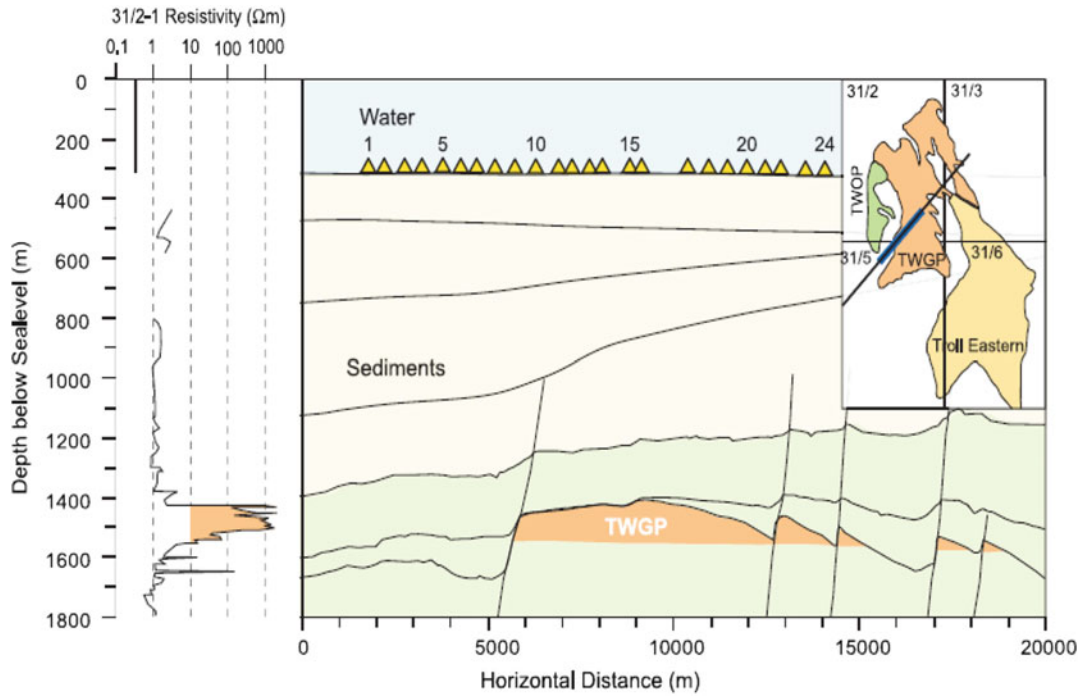

Fig. 20.16 Geological section across Troll West Gas Province (TWGP) together with resistivity data from exploration well 31/2-1. Outline of field and survey layout is shown on inset map. Thin line is towline for CSEM source and thick line indicates approximate position of CSEM sea floor receivers

The geological models and results from the modelling are shown in Fig. 20.17. Average resistivity (Ωm) values used in the modelling are based on available well information. A TWGP reservoir resistivity of 250 Ωm is calculated from trimmed mean resistivity values from well 31/2-1 (Fig. 20.16). There is a strong increase in simulated CSEM response above TWGP along the selected survey line. The modelled response also increases with increasing reservoir width, and for 5 km width the simulated response is more than three times stronger than the response from a non-reservoir case.

20.4.3 Results and Interpretation

The survey was acquired in 2003 and designed with 24 EM receivers across TWGP as illustrated in Figs. 20.16 and 20.18. Data quality had reliable information to an offset of c.8 km. Normalised values of electric magnitudes vs. offset measured by two representative receivers, one above (ON) the HC accumulation and one outside (OFF) the HC accumulation, are shown in Fig. 20.18. The selected ON and OFF receivers record near identical magnitudes out to 3.5 km, but between 3.5 and 9.0 km offset the ON receiver shows systematically higher magnitudes compared to the OFF receiver. The corresponding normalised MVO predicted from forward modelling is also shown in the figure and there is good agreement between the forward simulations and the measured MVO values. Normalised MVO data for the OFF receiver are close to 1.0 which is in accord with subsurface sediments comprising only water-wet lithologies along this line segment.

Normalised MVO data for the ON-receiver are close to 1.0 out to ca 3.5 km but increase gradually to levels above 3.0 at 7.5 km offset before gradually decreasing with higher offset. Magnitudes measured by the ON-receiver are reasonably similar to the modelled response for TWGP, and in accordance with the position of this line segment over the main gas accumulation (Fig. 20.18).

In order to display CSEM sounding systematics along the entire survey line, median normalised magnitudes were calculated at 6.5 ± 0.5 km offset

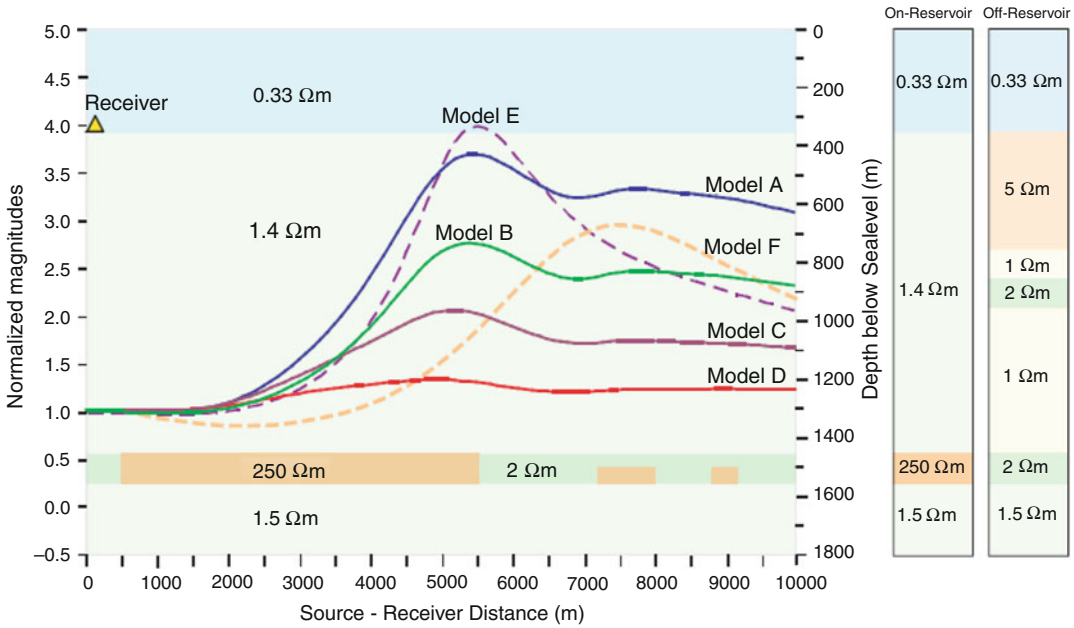

Fig. 20.17 Modelled CSEM responses from simplified Troll geological models. Columns to the right show plane-layer geological models representing ON and OFF reservoir situations. The differences in overburden resistivity between ON and OFF reservoir are due to lateral lithological changes. The cross-section is a modification of the east-west cross-section in Fig. 20.16. Results from both 3D modelling (*solid lines*) and plane-layer modelling (*dashed lines*) are included. Models A, C and D are responses from varying reservoir widths (5 km, 2.5 km and 1.25 km respectively). In model B the width increases from 3.5 km (*left*) to 5 km (*right*), representing an oblique crossing of Troll reservoir. Models E and F are responses from plane-layer modelling

for all receivers. This intermediate offset interval records close to maximum difference in measured magnitudes ON and OFF TWGP. Median normalised magnitudes at 6.5 ± 0.5 km offset for all receivers are illustrated in Fig. 20.18, with data plotted at 3.25 km offset halfway between source and receivers. Median normalised magnitudes are around 1.0 south west of TWGP (OFF), increase gradually up to 2.7 over the apex of the HC accumulation (ON), and decrease gradually down to 1.2 over the northwestern fringes of the field. The gradual increase is caused by the fact that both source and receiver must be above the target to record maximum returned energy from the HC accumulation. For TWGP this is the case only for a narrow zone above the middle part of the HC accumulation. We also see that the western slope of the anomaly is steeper than the eastern. A likely explanation for this is the asymmetric shape of the accumulation with a fault termination at the western extension and a more gradual eastward thinning as shown in Fig. 20.18. There are no observations of high resistive strata or structures that we know of, other than the TWGP, which can explain the high resistivity values measured by the survey. Due to extensive seismic surveying and drilling in this part of the North Sea, the geology of the area is very well known.

20.5 Gulf of Mexico Case Study

CSEM data and seismic data measure different Earth properties. The CSEM method is sensitive to resistivity variations, while the seismic method is sensitive to velocity and density variations. Both methods are therefore indirectly sensitive to HC saturation in a reservoir. The seismic method can normally see deeper into the subsurface than the CSEM method. It is always important to control that the measured targets are well inside the detectability range for the method used. Especially for the CSEM method sensitivity studies should always be performed to check if the actual prospect is within reach of the method.

Seismic velocity will have a sharp decrease when introducing even small amounts of gas in a water-filled sandstone reservoir. Since oil has comparable velocities to saline water the velocity effect is much

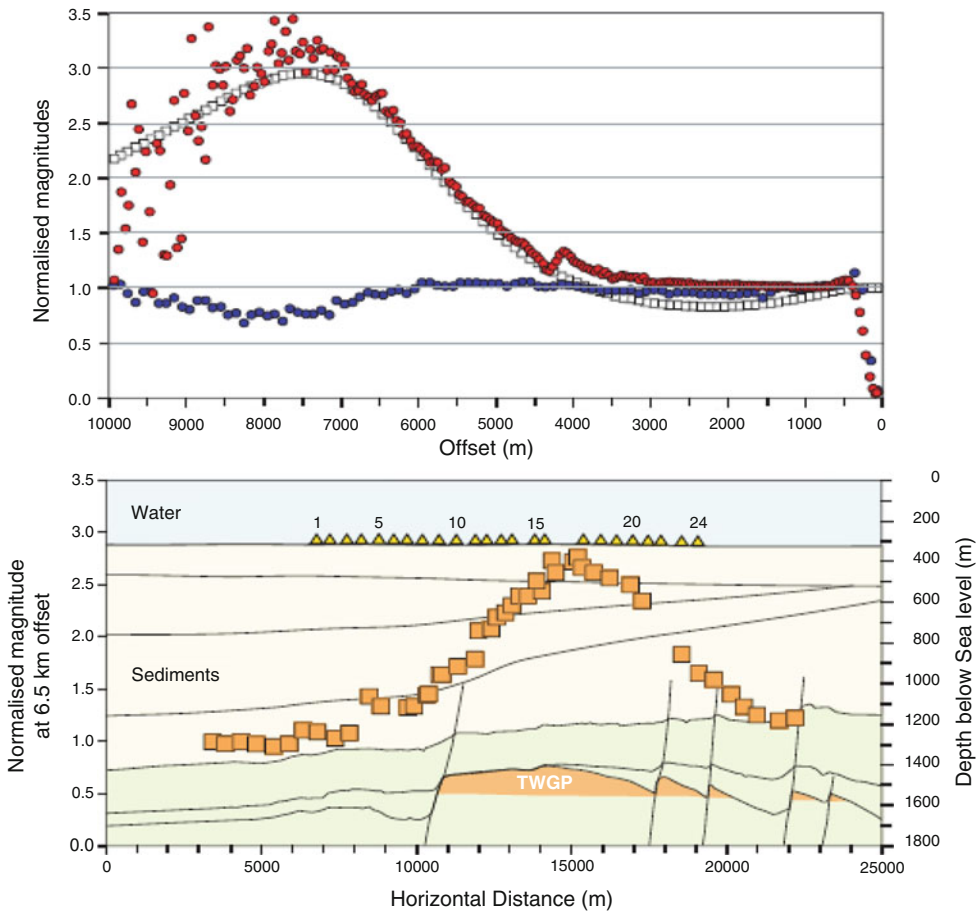

Fig. 20.18 (*Top*) Modelled and measured CSEM receiver data across Troll. *Red curve* represents a typical response from a receiver measurement ON the reservoir (Rx 24) divided by a (normalised) reference receiver OFF the reservoir (Rx 2). The source was towed SW-NE and shown responses are on the SW in-towing side of both receivers. *Blue curve* is the reference receiver normalised by the modelled plane-layer response representing the OFF reservoir situation. White curve is the modelled ON reservoir response normalised by the modelled OFF reservoir response. (*Bottom*) Median normalised magnitudes at 6.5 ± 0.5 km source-receiver distances along the survey line across Troll. Normalised magnitudes are posted at common midpoints 3.25 km from receivers. For better visualisation median magnitudes are overlain on the simplified geological model along the survey line. The correlation between the location of the CSEM anomaly and the Troll reservoir is excellent

smaller if oil, instead of gas, is present in the reservoir. If a HC-saturated reservoir is to be detected by the CSEM method the hydrocarbon saturation has to be high. It must reach 40–60% before the resistivity will significantly increase (Fig. 20.19) and the reservoir can be detected by CSEM sounding. Oil and gas will have similar effects and both will increase the resistivity in the reservoir. As a result of this it is challenging for the CSEM method to distinguish between different HC phases in the subsurface.

The relationships and properties mentioned above have implications for interpretation of a given HC prospect. If both seismic data and CSEM data show indications of increased hydrocarbon saturation the chance to find a reservoir with hydrocarbons is significant. If only the seismic data shows indication of hydrocarbon the chance to find a high saturation reservoir is reduced. The evaluation will depend on the expected fluid response in the seismic data. If only the CSEM data shows indications of high resistivity, with no hydrocarbon indications in the seismic data, lithology and other non-HC interpretations should also be carefully evaluated.

This Pemex case study demonstrates how seismic- and CSEM data can be used as a combined DHI tool for better HC prediction. The prospect is located in

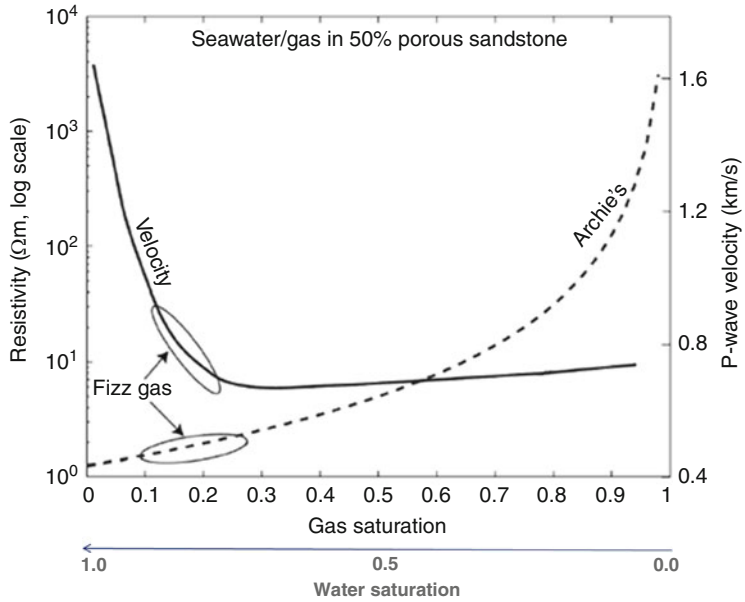

Fig. 20.19 P-wave velocity and resistivity as a function of hydrocarbon saturation (modified from Constable 2010). Acoustic p-wave velocity is sensitive to small volumes of gas in the porewater, but not very sensitive to further increasing gas saturation. Introducing oil instead of water in the pore space only has a moderate impact on p-wave velocity. Resistivity shows a large increase for low water saturation (high hydrocarbon saturation). Note that the resistivity curve is logarithmic. Commercial hydrocarbon reservoirs typically have water saturation lower than 0.4. The curves show that it is possible to differentiate low saturated hydrocarbon reservoirs from high saturated hydrocarbon reservoirs by combining seismic and CSEM data

deep water in the Gulf of Mexico. The trap is an anticline structure with a well-known regional reservoir interval approximately 700 m below the mud line. The prospect is covered by both 3D seismic and 3D CSEM data.

A seismic amplitude anomaly defines the maximum extent of the prospect, and a seismic flat spot defines a possible internal gas/fluid contact (Fig. 20.20). One possible model explaining these seismic observations is that the flat spot represents the gas/oil contact, and that the seismic amplitude anomaly below the flat spot is caused by presence of oil in the reservoir.

From the 3D inverted CSEM data we see that a resistive anomaly is consistent with the outline of the seismic flat spot (Fig. 20.21). There is no CSEM anomaly associated with the seismic anomaly below the flat spot. The combined DHI observations are interpreted to be due to variation in hydrocarbon saturation within the prospect. The crest of the structure was interpreted to have high saturation gas as there is a strong DHI indicator in both the seismic- and CSEM data. The lower part of the structure was interpreted to have low hydrocarbon saturation as there is no resistive anomaly associated with the seismic amplitude anomaly.

This combined seismic and CSEM interpretation was confirmed by a well showing high gas saturation and good reservoir sand at the top of the structure down to the flat spot. The same sand was also identified in an appraisal well down-dip on the structure, but here the reservoir sandstone had low hydrocarbon saturation as predicted in the interpretation.

20.6 Barents Sea Case Study

This case study shows how the combination of 2D seismic data and 3D CSEM data can be interpreted and used in exploration. 3D CSEM data covers the Johan Castberg field (Skrugard and Havis discoveries) on the Polheim sub-platform in the Barents Sea (Fig. 20.22). The survey also includes the exploration well 7219/9-1 to the southwest of the field. The Skrugard and Havis discoveries made in 2012 were based on observations on 3D seismic data (double flat

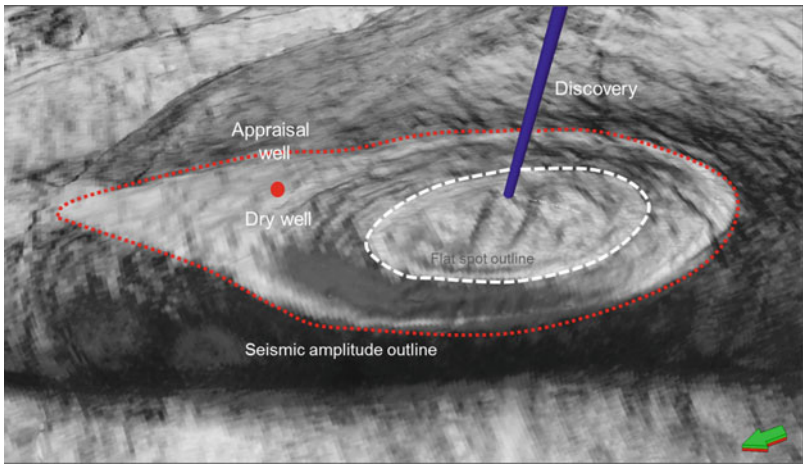

Fig. 20.20 Seismic depth slice showing outline of seismic anomaly (*red dotted line*) and flat spot (*white dotted line*). A seismic amplitude anomaly defines the maximum extent of the prospect, and a seismic flat spot defines a possible internal gas fluid contact. One possible model explaining these seismic observations is that the flat spot represents the gas/oil contact, and that the seismic amplitude anomaly below the flat spot is caused by presence of oil in the reservoir. Data courtesy Pemex

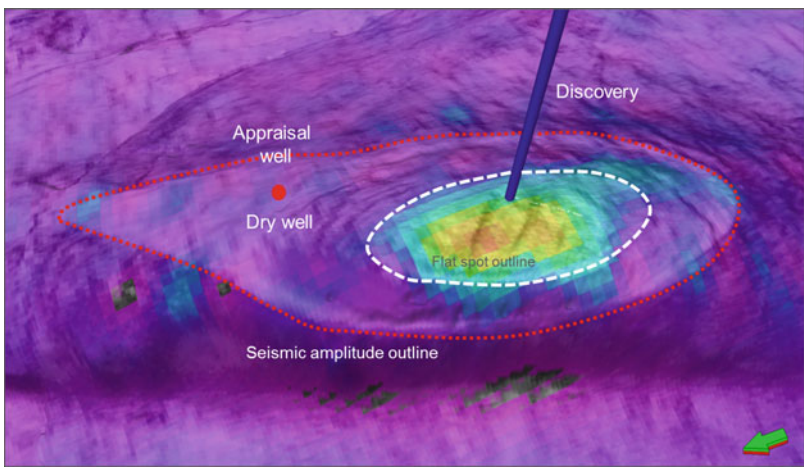

Fig. 20.21 Inverted resistivity data overlain seismic depth slice from Fig. 20.20. From the 3D inverted CSEM data we see that a resistive anomaly is consistent with the outline of the seismic flat spot (*blue-yellow-red colours*). There is no CSEM anomaly associated with the seismic anomaly below the flat spot (*pink colours*). The combined DHI observations are interpreted to be due to variation in hydrocarbon saturation within the prospect. Included are the positions of the gas discovery well and a low saturation gas appraisal well. Data courtesy Pemex

spot), but CSEM data also played an active role in evaluation of the prospects. The case example shows how CSEM data can detect the hydrocarbons in place and distinguish between the dry well (7219/9-1) and the discovery wells. It is therefore an excellent case to be used as a reference for further work in similar play models in the area.

The CSEM data was acquired in 2008 as a 3D survey where receivers were placed in a coarse grid on the seabed with a spacing of 3 km. The source was towed over each receiver line in a south-north orientation. The coarse receiver grid was used to effectively scan a large area and is typically used in frontier areas where limited information is available. Here the acquisition geometry was designed to cover a given area, and was not based on prospect outlines. Such a coarse receiver spacing will put some limitations on the target size that the CSEM data are able to detect. Ideally the

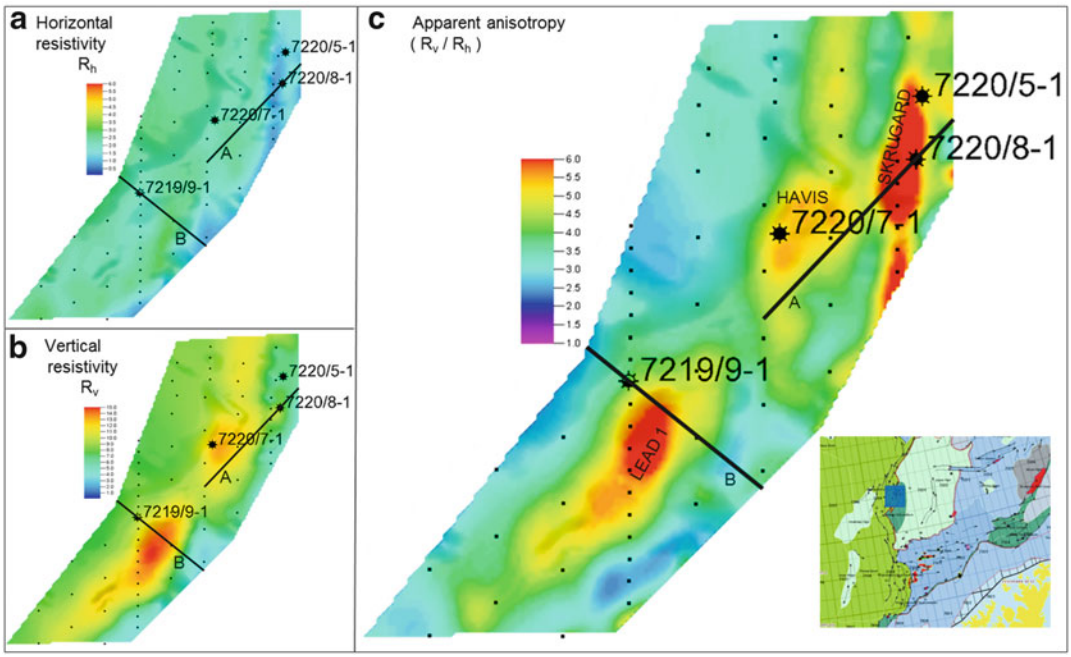

Fig. 20.22 Average CSEM maps from unconstrained 3D inversion calculated in a window 500 m above to 500 m below the Base Cretaceous unconformity. (**a**) Horizontal resistivity, R_h, (**b**) Vertical resistivity, R_v and (**c**) Apparent anisotropy. *Black squares* are receiver positions. Solid lines A and B show line location for seismic lines in Figs. 20.23 and 20.24. The *blue square* in the small overview map shows survey location in the Barents Sea. Data courtesy EMGS

prospects that can be detected should be within size for a commercial discovery in the region. In the Barents Sea such CSEM grids are actively used by oil companies for licencing round exploration, and also in some cases for drilling decisions.

Identifying prospective areas based on CSEM data alone is challenging. Also 2D seismic data will have its limitations due to coarse coverage and possible imaging problems. However, the combination of the two data types can be a powerful tool in exploration. Seismic data is used for geological understanding, structural mapping, play development, and to map prospect outlines. Resistivity trends and anomalies observed in the CSEM data can be better understood when integrated with seismic data. In this way, lack of 3D seismic information can to some extent be compensated for by the 3D resistivity information obtained from CSEM data. The EM data can also, in some cases, carry structural and geometric information that can guide the interpretation between the seismic 2D lines. Once a prospective area has been identified on seismic, 3D CSEM data can be used to upgrade or downgrade prospects. CSEM data can also generate new leads and prospects not yet identified by the seismic. Especially stratigraphic traps are often difficult to identify on seismic data.

In 1988 well 7219/9-1 was drilled at the crest of a fault block with main targets in Jurassic sandstones (Stø, Nordmela and Tubåen formations). A total thickness of 350 m of sandstones was encountered with porosities ranging from 16 to 18%. In addition, a thinner section of sand in the Lower Cretaceous section was found (Knurr formation). The well was dry with oil shows. Some years later Statoil made the two new discoveries, Havis and Skrugard, in a similar play model further to the northeast (Fig. 20.22).

When interpreting 3D CSEM data it is useful to extract resistivity maps centred on target horizons in order to get a lateral overview of resistivity variations and anomalies. As explained in Chap. 2, a horizontal resistivity (R_h) map will provide information about the regional trends, while a vertical resistivity (R_v) map will show regional trends as well as thin horizontal resistors (potential hydrocarbon reservoirs). A map of the anisotropy attribute (R_v/R_h) can also be created. Such a map will show the regional anisotropy, but will

in addition highlight areas where thin horizontal resistors are present.

In Fig. 20.22 resistivity maps (R_h and R_v), and anisotropy map created from unconstrained inversion of 3D CSEM data, are shown. All maps are calculated with a 1,000 m wide window centred on the Base Cretaceous unconformity. The horizontal resistivity map shows the regional resistivity trend in the data. This is also the case for the vertical resistivity map, but in addition two distinct anomalies appear. One is at the location of the Havis discovery, and the other (Lead 1) is southeast of Well 7219/9-1. Only a very weak anomaly is associated with the Skrugard discovery well 7220/8-1.

Figure 20.22c shows the apparent anisotropy. In this map three main anomalies are clearly observed. Havis and Lead 1 are already identified in the vertical resistivity map. In addition the Skrugard discovery is now identified as a strong anomaly. The Skrugard and Havis discoveries are located in rotated fault-blocks in Early to Middle Jurassic sandstones. Figure 20.23 shows a line crossing the Skrugard discovery well. Overlying the seismic data is the apparent anisotropy attribute and the position of the discovery well. The resistivity anomaly is located at the crest of the fault block and correlates with the Skrugard HC discovery. Here, CSEM data has the potential to increase the seismically determined chance of success as the CSEM anomaly correlates with the location of the prospect. The rotated fault block drilled by well 7219/9-1 (Fig. 20.24) does not show a resistive anomaly at the crest of the fault block. This well was drilled on a similar play model as the Skrugard and Havis discoveries, but was a dry well. This combination of subsurface responses from the discoveries and the dry well can be used as calibration to de-risk similar prospects in the area where both seismic data and CSEM data are available.

Figures 20.22 and 20.24 show a resistivity anomaly east of well 7219/9-1 (lead 1). This anomaly is different from the Skrugard and Havis anomalies as it is not located at the crest of the fault block, but in a down-dip position. One possible interpretation of this anomaly is to couple it to a stratigraphic trap within the syn-rift deposits. It could also be explained by general lithology variations or possibly by the presence of

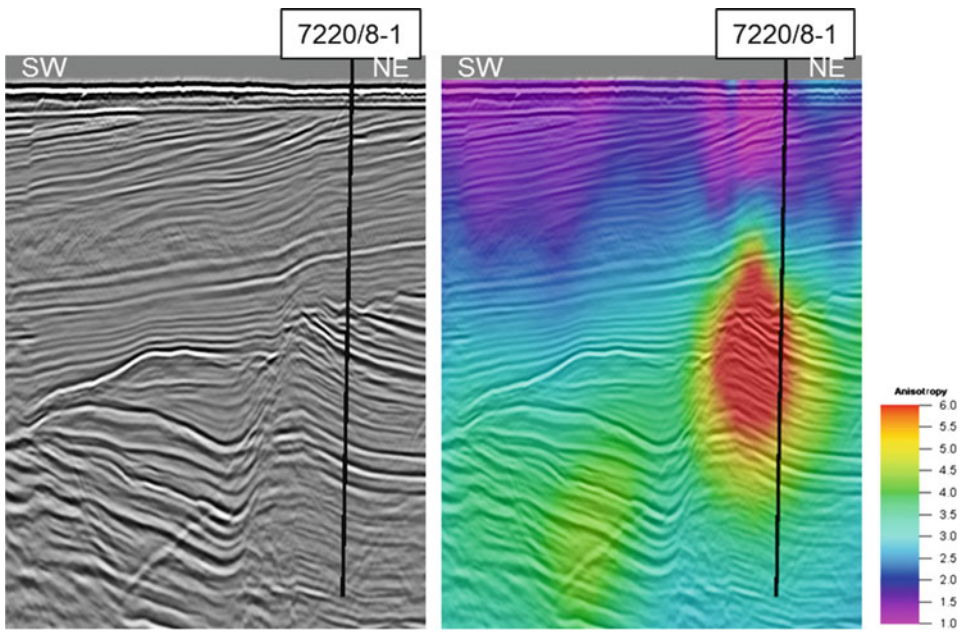

Fig. 20.23 2D seismic line (from MCG) and CSEM data (from EMGS) across the Skrugard discovery (Line A in Fig. 20.23). Overlain is the apparent anisotropy from the CSEM data and the well locations (*right*). The discovery sits at the crest of the rotated fault block where the *red* apparent anisotropy anomaly is seen

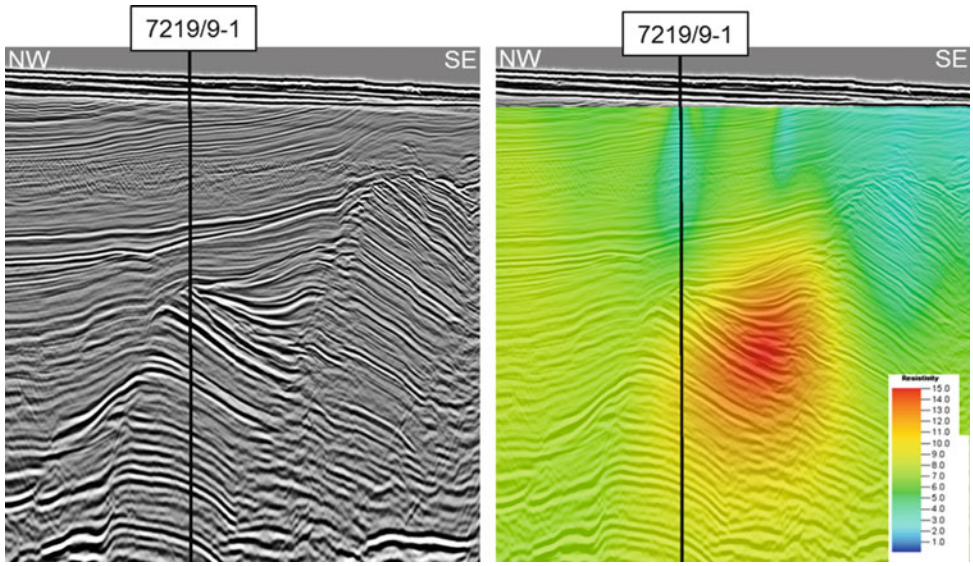

Fig. 20.24 2D seismic line (from MCG) and CSEM data (from EMGS) across the dry well 7219/9-1 drilled in 1988 (Line B in Fig. 20.23). Overlain is the vertical resistivity from the CSEM data and the well locations (*right*). The anomaly can be associated with a different play than the Skrugard and Havis discoveries. See text for explanation

organic-rich and resistive source rocks. More data is needed for a more detailed interpretation of this CSEM anomaly.

20.7 West of Shetland Case

20.7.1 Background

Due to the large velocity contrast between sediments and many basaltic rocks most of the acoustic energy is reflected and scattered back from basaltic layers. Therefore, seismic imaging of rocks beneath basaltic strata is difficult.

Basaltic rocks have high resistivities while water-wet sedimentary rocks have low resistivities. In resistive rocks the electromagnetic energy will be less attenuated compared to conductive rocks and the energy will penetrate deeper into the subsurface. This case example shows how the combination of CSEM, MMT and seismic data can improve interpretation of basaltic layers as well as deeper structures beneath the basalts.

In Paleocene times before continental break up between Greenland and Norway/Great Britain, the present day continental shelfs were situated next to each other Fig. 20.25. In Late Paleocene to Early Eocene times the break up was initiated, and a period with thermal uplift, massive volcanism, extension and subsequent seafloor spreading was initiated.

West of Shetland the volcanic complex consists of flow-basalts, volcanoclastics and intrusives. During deposition the complex advanced towards the east. Today it pinches out east of the Rosebank hydrocarbon discovery West of Shetland (Fig. 20.25). A typical succession consists of volcanoclastics at the base, a mix of volcanoclastics and flow basalts in the middle, and thick flow-basalts at the top. At the eastern edge the succession confluences with the Flett NW prograding delta creating the Rosebank play concept. In the Rosebank prospect the Flett delta is dominated by fluvial to marginal marine deposits.

Along the eastern edge, the thinnest part of the volcanic complex is to some extent known from seismic surveys and drilling. However, the gross distribution and nature of the inferred sedimentary basins beneath the volcanic complexes is not known. The reason for this is the mentioned problem the seismic technique has seeing through the basaltic complex and into the sedimentary succession below. Of particular interest is to map the thickness of the volcanic complex, and also to identify a possible transition from the inferred conductive sedimentary basin below the basalt to a deeper resistive basement.

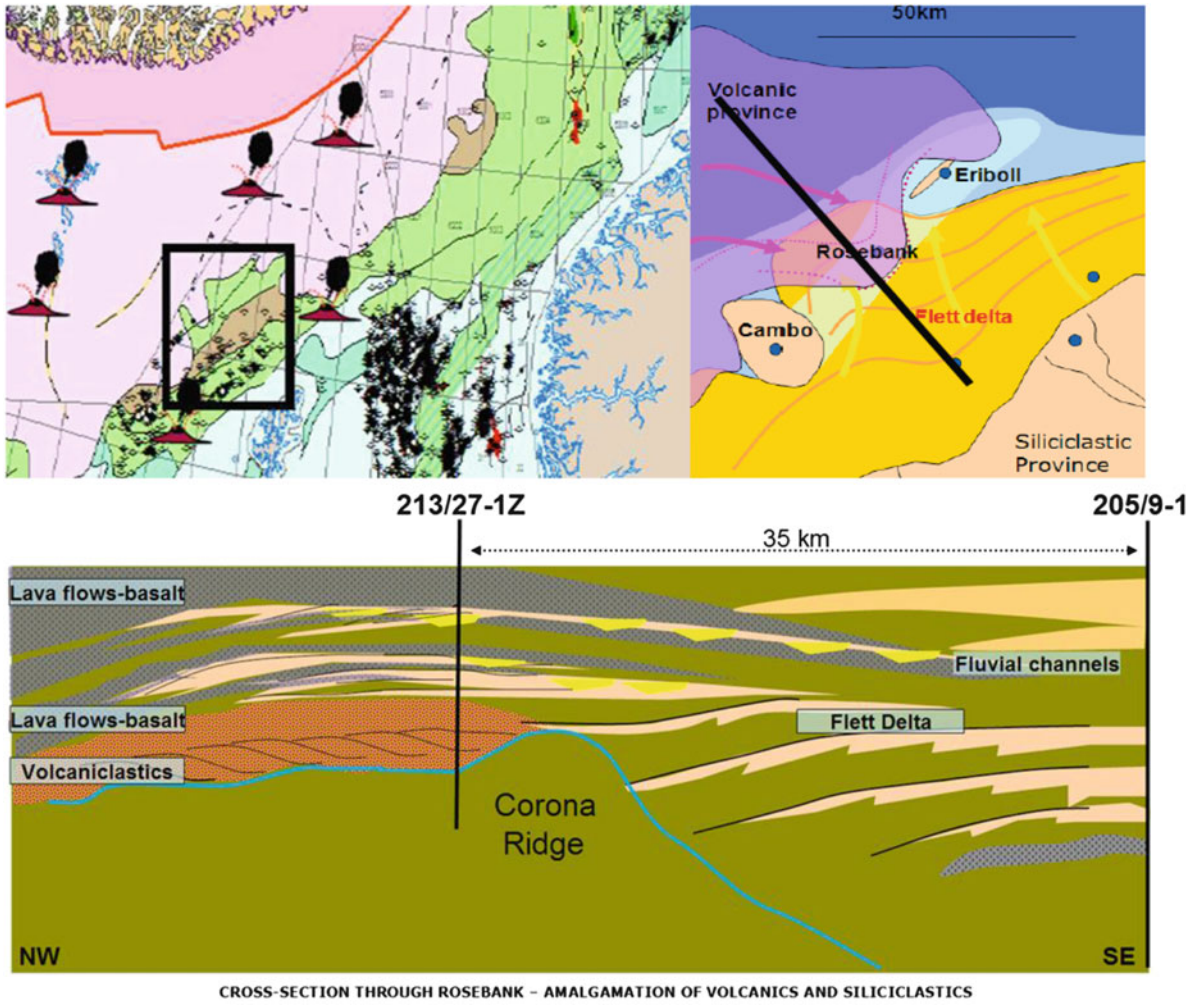

Fig. 20.25 (*Upper*) Pre break-up (Late Paleocene to Early Eocene) reconstruction of Greenland and Norway/Great Britain. Present day continental shelves were situated next to each other. (*Lower*) The volcanic complex pinches out east of the Rosebank hydrocarbon discovery. The complex consists of volcaniclastics and flow basalts. At the eastern edge the succession confluences with the Flett delta creating the Rosebank play concept. Location of profile is shown in the *upper right figure*

CSEM sounding is here used to map the electrical properties in the upper part of the succession, and MMT is used to map the deeper part. The electromagnetic data is acquired along a profile from the Rosebank Field in the UK sector to the Brugdan prospect in the Faroe sector (Fig. 20.26)

20.7.2 Results

Seismic data identifies the top of the basaltic complex quite well, but has problems identifying the base of the basalt as well as deeper structures. Where the basaltic layers are thin along the eastern edge, seismic data can to some extent see inside and through the complex. But this is not the case when the thickness increases in a westerly direction (Figs. 20.25 and 20.27)

Both the individually inverted results and the joint CSEM/MMT inversion results are shown in Fig. 20.27. The Inverted CSEM result images the basaltic complex quite well, but is hampered by attenuation in the inferred low resistive sedimentary rocks beneath the basalts. The transition from the overlying conductive sediments to the resistive volcanics, as well as the gradual thinning of the volcanic unit

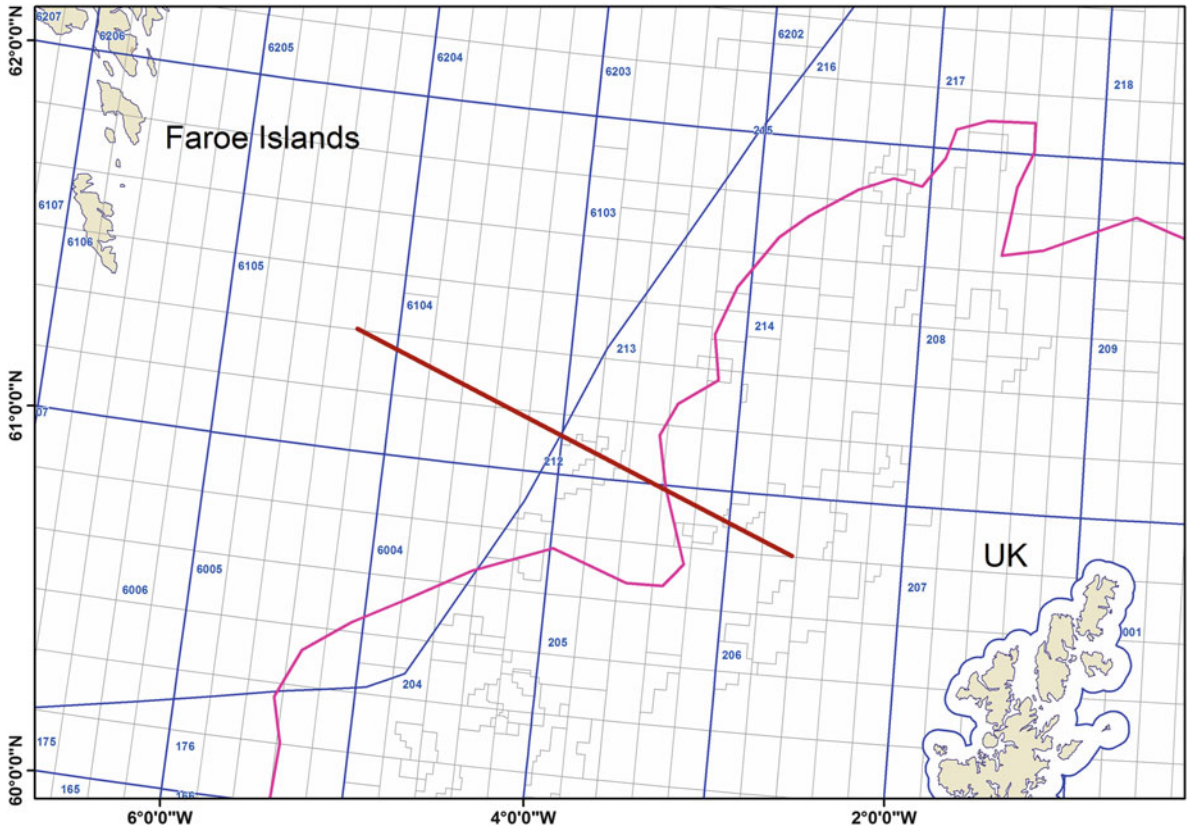

Fig. 20.26 Location of the combined CSEM/MMT Rosebank—Brugdan survey profile west of Shetland

towards the east, is very well imaged. The transition from resistive to conductive strata can be gradual. This in combination with gradual thinning of the resistive strata and general low resolution of the CSEM data makes it difficult to define the lateral edge precisely. The inverted MMT data has low resolution, but is able to define deep and large-scale structures. It is not able to define the shallower volcanic complex in any detail.

In the joint inversion result the total gross resistivity distribution is calculated. Two deep basin-shaped conductive structures separated by a resistive structural high are present along the EM section (Fig. 20.28). The low resistivity values below the basaltic complex are comparable to the values above the complex. This strongly indicates that sedimentary strata are present below the basalts. The strata are shaped as a low relief half graben bounded to the east by a resistive ridge. Further, based on the shape of the resistive bodies, the inferred basin could be bounded by larger-scale faulting (stepwise deepening) to the west, and more gradual shallowing towards the east. East of the ridge the data show significant deepening into another sedimentary basin. This conductive structure correlates with the position of the West Shetland Basin.

This case study is a very good example of how seismic-, CSEM- and MMT data can be combined to reveal structures in an area were the individual data set alone cannot resolve the problem.

20.8 Implications for HC Play- and Prospect Evaluation

EM methods' general ability to map electrical properties in the subsurface has proven very good. However, when using CSEM and MMT data for HC exploration it should be kept in mind that they are low resolution methods. Accurate depth estimation to resistive anomalies can also be a challenge. In addition, for the CSEM method, depth penetration is

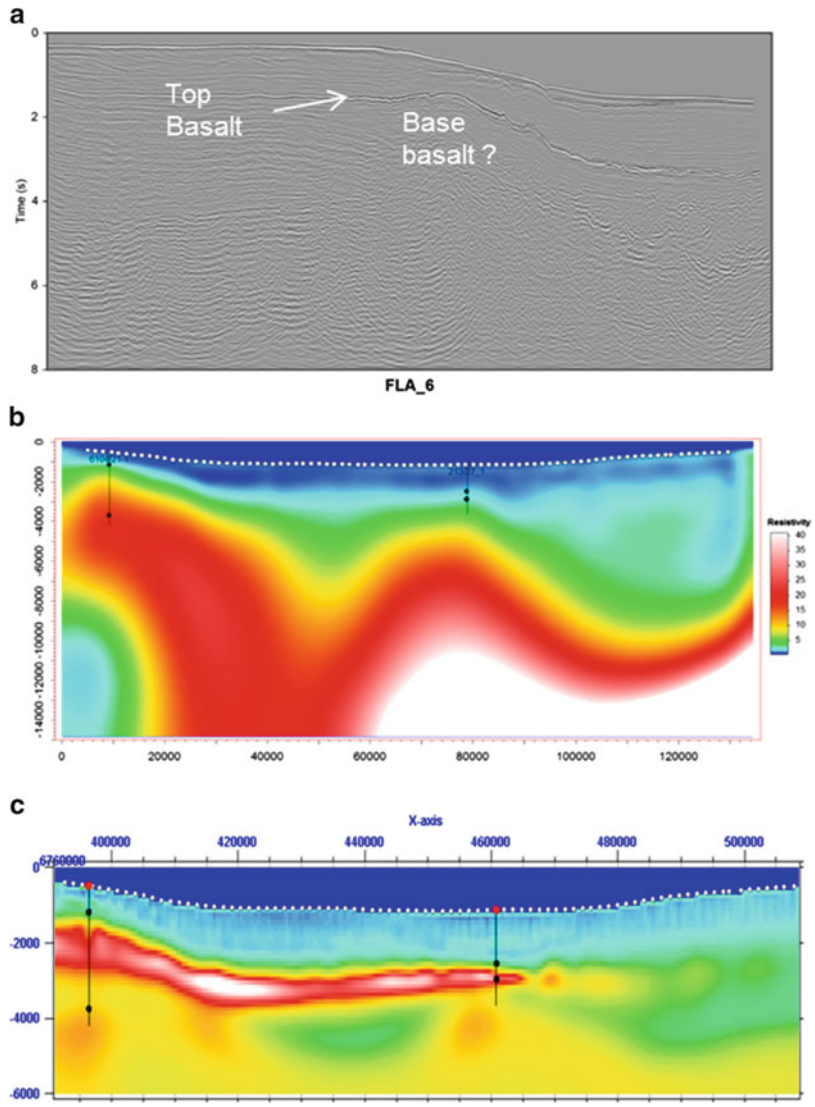

Fig. 20.27 2D seismic data (**a**), MMT inversion (**b**) and CSEM inversion (**c**). Seismic data identifies the top of the basaltic complex. It has problems identifying base of the basalts and cannot image strata below the basaltic layers. MMT data identifies large-scale structures. CSEM data identifies top and base of the basaltic complex, and to some extent also deeper structures. *Vertical black lines* (in Fig. **b** and **c**) show well positions and *black solid circles* are top and base of the basalts identified in the wells. MMT and CSEM data courtesy EMGS

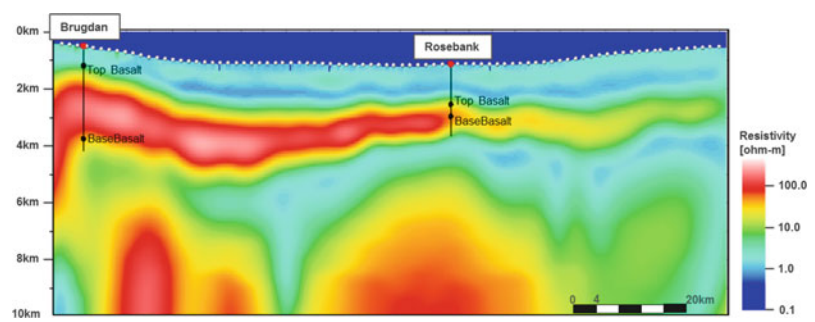

Fig. 20.28 In this joint CSEM- and MMT inversion both the deeper structures and the basaltic complex are identified. See text for discussion. Data courtesy EMGS

significantly smaller compared to the seismic reflection method.

For analysis of basins, petroleum systems, plays and prospects the individual HC companies have their own proprietary HC assessment methodology. The work flows are based on their experience, knowledge, data access, and method performance statistics. Today, seismic data and well data are the dominating data type. Here, we discuss the potential that electromagnetic data has for adding new and valuable information to the HC evaluation process. Offshore EM data has been available for some years, but it takes time to get enough experience to include a new data type in the evaluation process.

20.8.1 Basin Scale Analysis

A sedimentary basin can have one or several working petroleum systems, and a system can contain one or several petroleum plays. In a working petroleum system, source rock, reservoir rock and overburden rock must be present. In addition trap formation, hydrocarbon migration and accumulation must occur. Finally, the timing of events must also be correct.

In the case study from West of Shetland, seismic imaging of the potential sedimentary strata is hampered by the basalts covering the area. The inverted EM data shows a conductive unit below the resistive basaltic complex. This unit is interpreted as a sedimentary basin, and EM data can in this way improve the HC evaluation at basin scale. Gross depth, shape, size and electrical properties of the basin can be interpreted from the EM results.

If source rocks are present in the region, the interpreted EM data can give a first indication of potential for maturation and large-scale HC migration patterns. If information about heat flow and temperature gradients exist, theoretical oil and gas windows can be suggested for the interpreted basin.

The approximate thickness and shape of the resistive basaltic complex is also mapped. The base of the basalts is deepest in the centre of the basin and shallows gradually towards the basin margins. In this case, if the basaltic layers work as vertical fluid barriers, potential hydrocarbons could migrate towards the margins of the basin. The Rosebank discovery is situated in such a position (Fig. 20.28). Here, HC is found both in traditional sandstone reservoirs and in reservoirs with volcanic influence. Although the HC may have migrated from the Shetland Basin east of the basement high, these are all positive indications that the basin below the basalts could have a working petroleum system.

20.8.2 General Prospect Identification

To map out lateral variations in the electrical properties, 3D CSEM data is needed. Collecting both inline and broadside data enable measuring vertical and horizontal resistivity. When several EM anomalies are identified, from the resistivity measurement alone, it is difficult to know what is causing the various anomalies, and additional information is needed. In combination with seismic data, CSEM data can be used for prospect identification. Seismic is the superior tool for identification of structural traps, but to identify stratigraphic traps is a much more difficult task, and CSEM data can here give crucial additional information. In such a work flow CSEM is used as a general prospect mapping tool and not as a DHI tool. The mapped anomalies can have several interpretations other than subsurface hydrocarbons. These can be stratigraphic and lithological variations, structural topography, intrusives, extrusives, salt, carbonates or evaporites. When CSEM data is used in this way for prospect and lead identification within a play, in the end, the prospect must also be mapped on 3D seismic data to become a drillable prospect.

20.8.3 DHI Analysis

Since CSEM was introduced to HC exploration it has mainly been used as a direct hydrocarbon indicator. The method can then potentially influence the prospect ranking process. When it is used in this way it should always be used in combination with all available geophysical and geological data. In the cases described above, except for the West of Shetland case, the method has been used in this way.

One way to use the results from a CSEM DHI analysis in the risking process, is for modification of the original geological chance of success for the prospect.

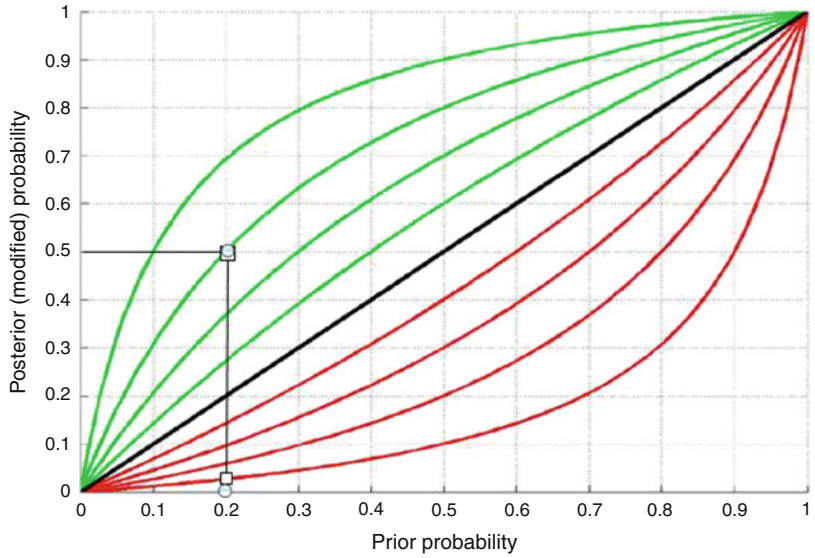

Fig. 20.29 Modification of geological risk by introducing CSEM data in prospect evaluation. By using performance tracking the prediction strength for the CSEM data can be quantified and used in the evaluation process. See text for explanation

To do this, information about prediction strength for the new data is needed. In this way the value of the new information can be quantified. When evaluating prediction strength, the strong and weak sides of the CSEM technique must be taken into consideration. On the strong side is the ability to measure general resistivity variations, areal distribution of the resistivity anomaly, and in some case also the thickness and volume of the measured objects. The ability to map these parameters is strongly dependent on acquisition geometry and complexity of the subsurface. The method's weak sides are for example vertical resolution, depth conversion and strong attenuation with depth.

Another important step in evaluating the prediction strength of CSEM data is to perform a thorough sensitivity study including detailed forward modelling. Further, statistical performance data for similar CSEM targets can be included and used in a risk modification procedure.

However, the lack of significant performance data is a challenge when using a relatively new data type like CSEM data. In the ideal case all relevant subsurface scenarios that can explain the CSEM observations should be included, also those not involving hydrocarbons.

However, the performance data base can be simplified, and the measured CSEM cases can be divided into two categories: *Right* prediction or *Wrong* prediction. Now, in a case were the geological chance of success for a prospect is decided, it can be modified by including CSEM data. If the *Right*/*Wrong* ratio from the performance data base is high the impact on the geological chance of success will also be high. Figure 20.29 can be used to illustrate the effect adding new information from CSEM data will have on a prospect's geological chance of success.

If it is decided that the geological chance of success for your prospect is 20%, it will plot at 0.2 on the horizontal axis. Your performance data base for the CSEM data have told you, that for the setting your prospect is in, the prediction strength is very good with a R*ight*/*Wrong* ratio as high as 0.8. The 0.8-line in Fig. 20.29 is green line number three up from the 0.5 black line. Then, if the acquired CSEM data are positive, the modified chance of success in this example would increase from 0.2 to 0.5. If the CSEM data are negative the modified probability should be decreased to approximately 0.06.

CSEM data can of course also be used without having a performance data base available, but as experience with the method builds up, this is one way to include the new knowledge in the prospect risking process. In many cases, for many companies, a statistical performance database is not available. In such

cases it is particularly important to integrate the CSEM information with all other geophysical and geological data available.

Acknowledgements We thank Rune Mittet for valuable comments on the manuscript, and we thank Pemex, MCG and EMGS for permission to use the data examples.

Further Reading

Alcocer, J.A.E., García, M.V., Soto, H.S., Baltar, D., Paramo, V.R., Gabrielsen, P., et al. 2013. Reducing uncertainty by integrating 3D CSEM in the Mexican deep-water exploration workflow. First Break 31(4), 75–79.

Bhuyian, A.H., Landrø, M. and Johansen, S.E. 2012. Three-dimensional modeling and time-laps sensitivity for subsurface CO_2 storage. Geophysics *77*(5).

Bhuyian, A.H., Thrane, B.P., Landrø, M. and Johansen, S.E. 2010. Controlled source electromagnetic three-dimensional grid-modelling based on a complex resistivity structure of the seafloor: effects of acquisition parameters and geometry of multi-layered resistors. Geophysical Prospecting 58, 505–533.

Bhuiyan, A.H., Wicklund, T.W. and Johansen, S.E. 2006. High-resistivity anomalies at Modgunn Arch in the Norwegian Sea. First Break 24, 39–44.

Buland, A., Løseth, L.O., Becht, A., Roudot, M. and Røsten, T. 2011. The value of CSEM data in exploration. First Break 29(4), 69–76.

Chave, A.D. and Cox, C.S. 1982. Controlled electromagnetic sources for measuring electrical conductivity beneath the oceans 1. Forward problem and model study. Journal of Geophysical Research 87(B7), 5327–5338.

Constable, S. 2010. Ten years of marine CSEM for hydrocarbon exploration. Geophysics 75(5), 75A67–75A81.

Constable, S. and Chester, J. 2006. Weiss Mapping thin resistors and hydrocarbons with marine EM methods: Insights from 1D modeling. Geophysics 71, G43–G51.

Cox, C.S., Constable, S.C., Chave, A.D. and Webb, S.C. 1986. Controlled source electromagnetic sounding of the oceanic lithosphere. Nature 320, 52–54.

Eidesmo, T., Ellingsrud, S., MacGregor, L.M., Constable, S., Sinha, M.C., Johansen, S.E., et al. 2002. Sea Bed Logging (SBL), a new method for remote and direct identification of hydrocarbon filled layers in deepwater areas. First Break 20, 144–152.

Ellingsrud, S., Sinha, M.C., Constable, S., MacGregor, L.M., Eidesmo, T. and Johansen, S.E. 2002. Remote sensing of hydrocarbon layers by Sea Bed Logging (SBL): Results from a cruise offshore Angola. The Leading Edge 21, 972–982.

Fanavoll, S., Ellingsrud, S., Gabrielsen, P., Tharimela, R. and Ridyard, D. 2012. Exploration with the use of EM data in the Barents Sea: The potential and the challenges. First Break 30(4), 89–93.

Gabrielsen, P. and Fanavoll, S. 2012. Application of CSEM data in exploration—A case study from the Nordland Ridge, Norwegian Sea. SEG International Geophysical Conference and Oil and Gas Exhibition, Istanbul. Extended abstract.

Gabrielsen, P.T., Brevik, I., Mittet, R. and Løseth, L.O. 2009. Investigating the exploration potential for 3D CSEM using a calibration survey over the Troll Field. First Break 27(6), 67–75.

Gabrielsen, P.T., Abrahamson, P., Panzner, M., Fanavoll, S. and Ellingsrud, S. 2013. Exploring frontier areas using 2D seismic and 3D CSEM data, as exemplified by multi-client data over the Skrugard and Havis discoveries in the Barents Sea. First Break 31(1), 65–73.

Hesthammer, J., Fanavoll, S., Stefatos, A., Danielsen, J.E. and Boulaenko, M. 2010. CSEM performance in the light of well results. The Leading Edge 29, 34–41.

Johansen, S.E., Amundsen, H.E.F., Røsten, T., Ellingsrud, S., Eidesmo, T. and Bhuyian, A.H. 2005. Subsurface hydrocarbons detected by electromagnetic sounding. First Break 23, 31–36.

Johansen, S.E., Amundsen, H.E.F. and Wicklund, Tor A. 2007. Interpretation of SeaBed Logging (SBL) data. Leading Edge, January Volume.

Johansen, S.E., Brauti, K., Fanavoll, S., Amundsen, H.E.F., Wicklund, T.A., Danielsen, J., et al. 2008. How EM survey analysis validates current technology, processing and interpretation methodology. First Break 26, 83–88.

Key, K.W. 2003. Application of broadband marine magnetotelluric exploration to a 3D salt structure and a fast-spreading ridge. Doctor of Philosophy thesis. University of California, San Diego.

Kong, F.N., Westerdahl, H., Ellingsrud, S., Eidesmo, T. and Johansen, S.E. 2002. Seabed logging: A possible direct hydrocarbon indicator for deepsea prospects using EM energy. Oil & Gas Journal, May 13.

Lu, X. and Xia, C. 2007. Understanding anisotropy in marine CSEM data. 77th SEG Annual Meeting, San Antonio.

Løseth, L.O. 2007. Modelling of controlled source electromagnetic data. Doctor of Philosophy thesis. Department of Physics at the Norwegian University of Science and Technology.

Mittet, R. and Gabrielsen, P.T. 2013. Decomposition in upgoing and downgoing fields and inversion of marine CSEM data. Geophysics 78, E1–E17.

Mittet, R. and Morten, J.P. 2012. Detection and imaging sensitivity of the marine CSEM method. Geophysics 77, E411–E425.

Mittet, R. and Morten, J.P. 2013. The marine controlled-source electromagnetic method in shallow water. Geophysics 78, E67–E77.

Morten, J.P. and Bjørke, A.K. 2010 Fast-track marine CSEM processing and 3D inversion. 72nd EAGE Conference & Exhibition incorporating SPE EUROPEC 2010, Barcelona. Extended abstract C004.

Morten, J.P., Roth, F., Karlsen, S.A., Timko, D., Pacurar, C., Olsen, P.A., et al. 2012. Field appraisal and accurate resource estimation from 3D quantitative interpretation of seismic and CSEM data. The Leading Edge 31, 447–456.

Weiss, C. and Constable, S. 2006. Mapping thin resistors and hydrocarbons with marine EM methods, Part II—Modeling and analysis in 3D. Geophysics 71, G321–G332.